Mississippi State University

Scholars Junction

12-10-2010

Microstructure-Based Multistage Fatigue Characterization And Modeling Of An Acrylonitrile Butadiene Styrene Copolymer

Jason Elvin Fountain

Follow this and additional works at: https://scholarsjunction.msstate.edu/td

MICROSTRUCTURE-BASED MULTISTAGE FATIGUE CHARACTERIZATION

AND MODELING OF AN ACRYLONITRILE BUTADIENE STYRENE

COPOLYMER

By

Jason Elvin Fountain

A Thesis
Submitted to the Faculty of
Mississippi State University
in Partial Fulfillment of the Requirements
for the Degree of Master of Science
in Mechanical Engineering
in the Department of Mechanical Engineering

Mississippi State, Mississippi

December 2010

MICROSTRUCTURE-BASED MULTISTAGE FATIGUE CHARACTERIZATION

AND MODELING OF AN ACRYLONITRILE BUTADIENE STYRENE

COPOLYMER

By

Jason Elvin Fountain

Approved:

_____
Mark F. Horstemeyer
Center for Advanced Vehicular Systems
Chair in Computational Solid Mechanics
Professor of Mechanical Engineering
(Major Professor)

_____
Jean-Luc Bouvard
Center for Advanced Vehicular Systems
Assistant Research Professor
(Committee Member)

_____
J. Brian Jordon
The University of Alabama
Department of Mechanical Engineering
Assistant Professor
(Committee Member)

_____
Youssef Hammi
Center for Advanced Vehicular Systems
Faculty
(Committee Member)

_____
David Marcum
Bille J. Ball Professor
Graduate Coordinator of the Department
of Mechanical Engineering
(Graduate Coordinator)

_____
Sarah A. Rajala
Dean of the College of Engineering

Name: Jason Elvin Fountain

Date of Degree: December 10, 2010

Institution: Mississippi State University

Major Field: Mechanical Engineering

Major Professor: Dr. Mark F. Horstemeyer

Title of Study: MICROSTRUCTURE-BASED MULTISTAGE FATIGUE
                 CHARACTERIZATION AND MODELING OF AN ACRYLONITRILE
                 BUTADIENE STYRENE COPOLYMER

Pages in Study: 60

Candidate for Degree of Master of Science

In this work, fatigue experiments and observations are used to experimentally and computationally quantify fatigue structure-property relationships and then capture these effects through a microstructure-based MultiStage Fatigue (MSF) model for a thermoplastic Acrylonitrile Butadiene Styrene copolymer. Completely reversed fatigue experiments were conducted over a range of strain amplitudes at two frequencies (1 Hz and 10 Hz). Scanning electron microscopy of fatigue fracture surfaces was used to quantify the microstructural notch root or initiating particle size for structure-property relations. Results were then processed in an MSF model sensitive to microstructural effects to capture the fatigue lifetimes for the thermoplastic ABS copolymer.

DEDICATION

I would like to dedicate this work to my extremely intelligent and beautiful wife

Carola, and to my Lord and Savior for continuing to bless me in every way imaginable.

ACKNOWLEDGEMENTS

Government or any agency thereof. The views and opinions of the authors expressed herein do not necessarily stat or reflect those of the United States Government or any agency thereof. Such support does not constitute an endorsement by TARDEC of the work or the views expressed herein. UNCLASSIFIED: Dist A. Approved for public release.

TABLE OF CONTENTS

LIST OF TABLES

LIST OF FIGURES

CHAPTER I

INTRODUCTION

Energy efficient design, particularly for automotive components using lightweight metal alloys and polymers, has become of great interest in the last decade. This heightened interest has encouraged further investigations into polymers within the materials science community for the polymeric material's ability to achieve needed strength and elongation properties, and more importantly, impact and fatigue resistance. As an increase in the application of polymeric materials for automotive structural and exterior components continues to climb, there is an amplified significance on the need for models capable of producing highly reliable fatigue predictions of the material.

The ability to capture the effects of polymer fatigue through modeling and simulation is important in understanding long-term reliability in automotive structural applications. Furthermore, the long-term reliability of polymers in fatigue is currently not well understood; consequently, modeling of polymer fatigue is lacking in literature. There is also a current lack of multiscale material models that are physics based as most are instead empirically based. These models can predict experimental results for limited tests; however, when the models are used for another material or tests, they cannot capture the response of complex stress state tests such as creep and fatigue.

Many empirically-based theoretical models, have been developed to evaluate the nature of glassy polymers with the primary objective of characterizing the mechanical behavior [Christensen, 1982; Krempl, 1995; Bardenhagen et al., 1997; Tervoort *et al.*, 1998; Tervoort and Govaert, 2000; Govaert et al. 2000; Van der Sluis *et al.*, 2001; Khan and Zhang, 2001; Lubarda et al., 2003; Khan et al., 2006]. In depth reviews on phenomenological models for glassy polymers have been developed in the literature [Chaboche, 1997; Bardenhagen *et al.*, 1997; Frank *et al.*, 2001; Zairi *et al.*, 2007]. These phenomenological models showed their ability to capture inelastic behavior of polymeric materials for a range of specific loading cases; however, the models lacked important microstructural properties and consequently were deficient in the ability to model history effects. As discussed by Ames *et al.* [2009], these models were developed through macroscopic testing results and generally fail in the prediction of micromechanical testing. Exclusion of micromechanical testing and features complicates the application of the phenomenological models in multiscale modeling. A more recent review of multiscale modeling of amorphous polymers by Bouvard *et al.* [2009], discussed the current state of literature as well as the challenges for the different length scales.

The physically-based models capture detailed mechanical response by inclusion of internal microstructure-property relations of the material [Haward *et al.*, 1968; Williams *et al.*, 1977; Boyce *et al.*, 1988]. Van der Giessen *et al.* [1999] developed a model which attempts to capture the two primary failure mechanisms of crazing and shear yielding. The model was then used to predict the competition of these mechanisms through the growth of a mode I crack. Although most of these models accurately characterize the mechanical properties of polymeric materials for most simple loading

cases, the models typically cannot capture the mechanical response when submitted to complex or cyclic loading cases.

A study on the fatigue crack growth of polymers by Radon [1980] summarized how the complexity of polymer fatigue mechanisms and an apparent lack of literature, and although there is a better understanding of molecular structures, physical behavior, and degradation mechanisms; the complexity of polymer fatigue is just as challenging to this day.

Empirically-based and physically-based models for fatigue of glassy polymers exist but are still lacking in literature. Kim *et al.* [1994, 1995] developed an empirically-based fatigue model that includes temperature and frequency effects for predicting crack growth rates in ABS. Pijnenburg *et al.* [2005] combined and compared micromechanical models for crack tip plasticity in polymer-rubber blends, and show the understanding of some important micromechanisms such as particle cavitation, void growth, crazing, and shear yielding is still lacking description in the polymeric models. Another model by Janssen *et al.* [2008] uses an elasto-viscoplastic model to capture fatigue life of polycarbonate and attempts to incorporate heat dissipation. These models typically capture the fatigue crack growth behavior for long crack regimes but ignore microstructure influence and disregard the three regimes of fatigue life: incubation, microstructurally small crack, and long crack.

Historically, the MultiStage Fatigue (MSF) model has considered the three regimes of fatigue crack growth and the microstructural features of metal alloys [McDowell *et al.*, 2003]. Features including but not limited to: grains, dendrite cell size, and nearest neighbor distance and size of inclusions (particles and voids) were admitted

3

into the MSF model; however, the complexity of polymers includes many structures and degradation mechanisms not attributed to metals: various forms of crosslinking, preparation sensitivity in terms on injection temperature, annealing techniques, and mold temperature effects [Pitman *et al.*, 1980; Lawandy, 1980a,b]. In general, polymers are also more susceptible to thermo-mechano-chemical degradation when compared with most metals. The components of ABS are poor thermal conductors leading to hysteretic heating and reducing the material's modulus and although the microstructural feature variability, processing sensitivity, and sensitivity to frequency and temperature effects. Due to the greater sensitivity these effects have on polymers, polymeric materials are generally considered much more complex in comparison to most metal alloys; however, there are some similarities which can reduce the gap between the two material families.

The copolymer used in this study, Acrylonitrile Butadiene Styrene (ABS), is formed by grafting polybutadiene elastomer to an Acrylonitrile Styrene matrix. For the ABS thermoplastic copolymer, there are two primary modes of failure: shear yielding and crazing [Sikka, 1980; Donald *et al.*, 1982; Van der Giessen *et al.*, 1999; Estevez, 2000]. Shear yielding in thermoplastics is plastic deformation through shear banding which can be attributed to the softening after global yield. Shear yielding typically occurs in compression where there is shrinkage in volume; whereas crazing is dominant in tension or an expansion in volume [Pijnenburg, 1999; Estevez, 2000; Tijssens, 2000]. Crazing is the nucleation of voids that do no coalesce, but rather form fibrils which stabilize a region [Estevez, 2000]. The formation of crazes generally appears as a stress whitened region, attributed to light scattering by the crazes, due to large deformation within the polymeric material [Donald, 1982]. Upon continued loading, the fibrils break down to form a crack.

In general, crazing is separated into three regimes: initiation, widening, and breakdown [Estevez, 2000; Tijssens, 2000]. Furthermore, the craze opening rate governs competition between the two primary failure mechanisms of shear yielding or brittle failure through craze formation and propagation.

The polybutadiene elastomer fillers act to toughen the ABS copolymer as these fillers demote crack propagation through craze blunting and promotion of shear yielding; however, as the filler content increases there is a reduction in overall stiffness [Seelig, 2002]. The bulk of the fillers generally introduced as toughening mechanisms for ABS range in size from 0.3 μm to 1.5 μm; however, defects, primarily composed of polybutadiene, of sizes greater than 100 μm have been found [Pijnenburg *et al.*, 1999; Marissen *et al.* 2001]. The cavitation of the smaller rubber fillers occurs in regions of high tensile stress and generally leads to shear deformation; whereas crazes tend to nucleate from larger particles [Donald *et al.*, 1982]. ABS copolymers with high contents of Acrylonitrile typically fail due to shear yielding and fracture attributed to craze formation. The dispersed polybutadiene inclusions encourage earlier craze growth and initiation; however, the inclusions lower crack growth rates within the Acrylonitrile Styrene matrix by blunting cracks. Both, the cavitation of smaller filler particles and concurrent shear yielding, and crazing are utilized in commercial ABS blends to help obtain desired toughness characteristics by incorporating both small and large particles [Donald *et al.*, 1982].

Studies on the micromechanisms of failure mechanisms and crack growth of glassy polymers show there are two primary types: normal fatigue crack propagation and retarded fatigue crack propagation [Konczol *et al.*, 1990; Adams *et al.*, 1993; Van der

5

Giessen *et al.*, 1999]. The normal type grows a steady crack where craze formation and growth is in unison with craze fibril tearing; whereas retarded fatigue crack propagation shows there may be many cycles of a crazed region prior to any crack advancement [Radon, 1980; Konczol *et al.*, 1990; Maiti *et al.*, 2005]. The current body of literature on these two primary competing failure mechanisms is quite extensive; however, the mechanisms are still not well understood. Consequently, microstructure-based fatigue modeling of thermoplastic polymers is also lacking in literature. Incorporating the microstructural features of metal alloys and polymers through a microstructure-based multistage fatigue model is a step towards bridging the gap between metals and polymers.

The MultiStage Fatigue (MSF) model, originally developed for aluminum alloys by McDowell *et al.* [2003], captures the effects of a given material's microstructure and reflects three regimes of crack growth [Suresh, 1998]; incubation (INC), microstructurally small crack or physically small crack (MSC), and long crack (LC), for both low cycle fatigue (LCF) and high cycle fatigue (HCF). This work focused on low cycle fatigue of the ABS copolymer.

In literature, the MSF model has been used to quantify the microstructural effect on fatigue life for many metal alloys including: a cast A356-T6 aluminum alloy [McDowell *et al.*, 2003], a die-cast AZ91E-T4 magnesium alloy [Horstemeyer *et al.*, 2004], a die-cast AM50 magnesium alloy [El Kadiri *et al.*, 2006], a cast AE44 magnesium alloy [Xue *et al.*, 2007a], cast A356-T6 and A380-F aluminum alloys [Xue *et al.*, 2007b; Jordon *et al.*, 2010], 7075-T651 aluminum alloy [Xue *et al.*, 2007c,d], a Laser Engineered Net Shaping (LENS) processed steel [Xue *et al.*, 2010], and most recently for an AZ61 magnesium alloy [Gibson *et al.*, 2010]; however, this is the first study on the

6

MSF model's ability to capture microstructural effects on the fatigue life of a non-metal material.

In this work, fully reversed uniaxial strain life experiments and observations were used to experimentally and computationally quantify fatigue structure-property relationships and then capture these effects through a microstructure-based MultiStage Fatigue (MSF) model for a thermoplastic Acrylonitrile Butadiene Styrene (ABS) copolymer. Completely reversed fatigue experiments were conducted over a range of strain amplitudes (0.005-0.05) at two frequencies (1 Hz and 10 Hz) to capture the low cycle regime of an ABS copolymer. Optical microscopy was used to quantify the size distribution of particles within the virgin material. Scanning electron microscopy (SEM) of fatigue fracture surfaces was used to quantify the microstructural notch root or initiating particle size for structure property relations. Results were then processed in a microstructure sensitive MSF model to capture the fatigue lifetimes for this particular ABS copolymer.

The purpose of this study is to experimentally quantify the fatigue behavior and the structure-property relationships of an ABS copolymer and then process this information through the microstructure-sensitive MSF model to capture fatigue behavior.

CHAPTER II

MATERIAL AND EXPERIMENTS

Material Characterization

The material used in this study is an engineering grade, high impact thermoplastic Acrylonitrile Butadiene Styrene (ABS) copolymer which is natural (beige) in color and produced by King Plastic Corporation. The ABS material, in pelletized form, was placed into a mold which was clamped closed followed by application of heat and pressure in which air is vented during processing. The mold was then cooled and the finished product was an industrial supplied 1" thick, 24" by 24" supplied plate used in this study.

The ABS material microstructure was first characterized using optical microscopy and SEM to quantify the virgin microstructure; however, further characterization of the as-received materials was performed to better document the material type used in this work for future collaborative studies. Figure 1 depicts the microtome used to prepare approximately 5 µm films for Fourier Transform Infrared Spectroscopy (FTIR) using a Nicolet 6700 FTIR to obtain absorbance profiles for the ABS copolymer. After cleaning and preparing the FTIR specimen stage, the polymer microfilms were placed on the FTIR for analysis as shown in Figure 2. The resolution of the 32 scans was set at 4, and the resulting absorbance plot for the ABS copolymer is shown in Figure 3.

Figure 1   A microtome was used to cut Acrylonitrile Butadiene Styrene copolymer specimens to approximately 5 µm thick films for Fourier Transform Infrared Spectroscopy experiments.
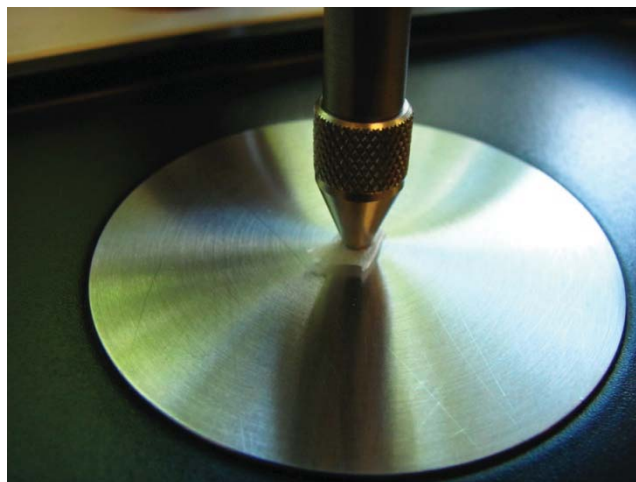
Figure 2   Fourier Transform Infrared Spectroscopy performed on an Acrylonitrile Butadiene Styrene copolymer micro-film using a Nicolet 6700 FTIR to obtain absorbance profiles.
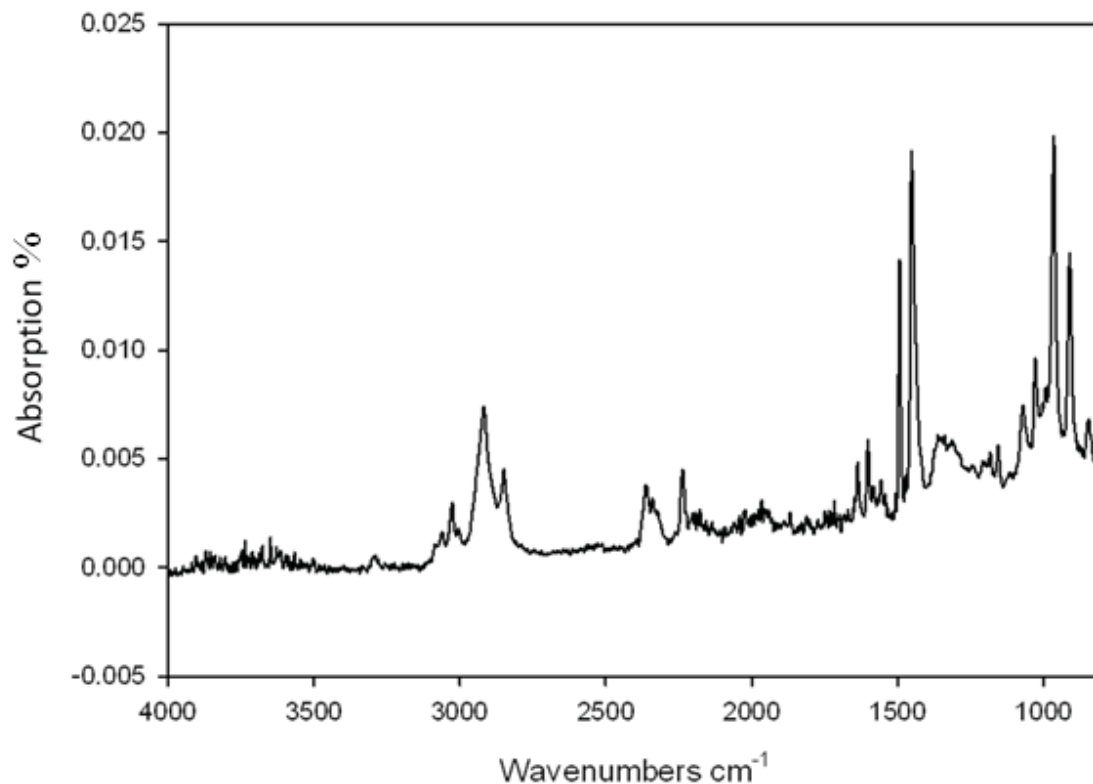
Figure 3   Fourier Transform Infrared Spectroscopy was used to obtain an absorbance
profile of the Acrylonitrile Butadiene Styrene copolymer for future
collaborative studies (32 scans at a resolution of 4 cm^{-1}).

Using the Nicolet FTIR, infrared light was passed through the microtomed ABS

specimens at differing angles to obtain the spectra shown in Figure 3.   The main

absorption bands for this particular ABS are approximately: 2360 cm^{-1} for Acrylonitrile,

960 cm^{-1} for 1,4-trans-butadiene, and 1400 cm^{-1} for styrene [Scheirs, 2000]. Comparison

of the spectra for ABS materials used in future work to the spectra above can help to

further determine how congruent the materials are for extension of this work.

Static and cyclic properties for the ABS copolymer are listed in Table 1.

Table 1   Static and cyclic properties of the ABS copolymer used in this study.

Young's Modulus E_i (MPa)	Yield Strength S_{yi}(MPa)i	Ultimate Strength S_i (MPa)i	Elongation (%)	Cyclic strength coefficient K`	Cyclic hardening exponent n`
2200	30.69	42.97	40	75	0.15

Monotonic Loading

Monotonic tensile and compression experiments were performed using an Instron 8850 load frame. An INSTRON 2630-110 extensometer was used and a feedback loop between the extensometer and the load frame was employed to ensure a constant engineering strain rate over the entire duration of each test. Figure 4 shows the tensile testing setup used for ABS specimens. Tensile specimens were tested over a range of engineering strain rates (0.001/s, 0.01/s, and 0.1/s) and over a range of temperatures (50˚ C, 25˚ C, and -20˚ C) to failure.
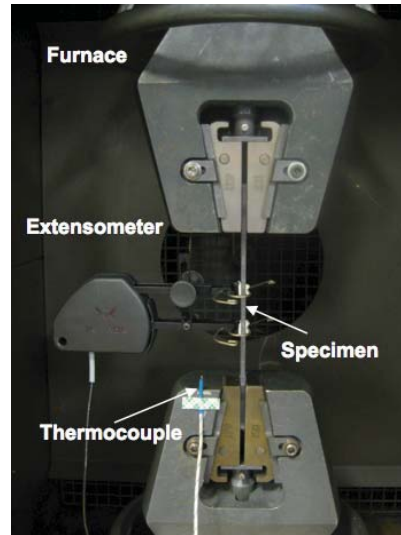
Figure 4   The experimental setup used for monotonic tensile tests of ABS specimens using an Instron 8850 load frame and an Instron 2630-110 extensometer.

Monotonic tensile specimens were made from the industrial supplied 1" plate of ABS via a Computer Numerical Control (CNC) machine, following the geometry proposed by ASTM D638-03 Type 1 specimens as shown in Figure 5.
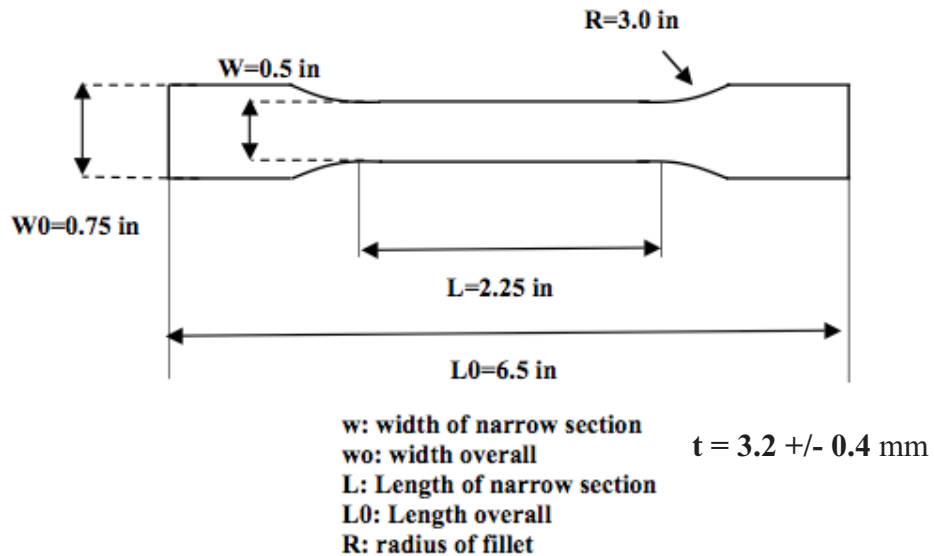
Figure 5   The flat dog-bone shaped tensile specimen geometry used for monotonic tension tests as per ASTM D638-08, Type 1 specifications.

Figure 6 shows the cylindrical compression specimen test setup in which an Instron 2630-110 extensometer was mounted to the compression platens to help eliminate compliance of the load frame and fixtures. Compression specimens were tested over a range of engineering strain rates (0.001/s, 0.01/s, and 0.1/s) and over a range of temperatures (110 C, 50 C, 25 C, and -20 C) from 0-100%-0 true strain.

Figure 6   The experimental setup used for monotonic compression tests using an Instron 8850 load frame and an Instron 2630-110 extensometer.

Tests at -20° C and elevated temperatures were performed using an INSTRON Environmental Chamber 3119-407 shown previously in Figure 5. A thermocouple positioned close to the specimen was used to ensure a constant temperature upon heating or cooling.

For the compression tests, two types of moly-paste lubricants supplied by Dow Corning were used on the compression specimens and compression platens which helped to further minimize friction and specimen barreling and allowed uniaxial loading to be obtained. A G-n Molykote assembly lube was used for tests below room temperature, and a Rocol dry moly-paste was used for tests performed at room temperature and above. Prior to beginning the test, a small preload of 0.5 MPa was applied to each specimen to ensure full contact of the platens with the specimen, and also to reduce the affect of the

compression of moly-paste on the data. A separate study verified that the preload applied does not change the mechanical response of the materials.

Monotonic compression specimens were cut from the industrial supplied 1" thick plates in the form of right cylinders, as shown in Figure 7, via CNC with a diameter of 12.7 mm and a length of 6.35 mm which corresponds to a 1:2 length-to-diameter ratio and follows a similar geometric ratio used for thermoplastic polyurethane by Qi *et al.* [2004], which helps to prevent barreling of the specimens.

Figure 7   Cylindrical compression specimens with a 12.7 mm diameter and a 1:2 length/diameter ratio were used for monotonic compression tests (shown prior to polishing).

Fatigue

Fully reversed uniaxial cyclic testing was performed using an MTS 810 servo-hydraulic load frame, as shown in Figure 8, in an ambient laboratory environment. An MTS model 634.31F-25 axial extensometer was used for strain controlled tests. The cylindrical dog-bone shaped specimens were tested until failure at two frequencies (1 Hz

and 10 Hz) and over range of strain amplitudes (0.005, 0.006, 0.007, 0.01, 0.02, 0.025, 0.028, 0.03, and 0.04).   Temperature generation was monitored using an Optris laser thermometer.

Figure 8   An Acrylonitrile Butadiene Styrene copolymer cylindrical dog-bone shaped fatigue specimen mounted in an MTS 810 servo-hydraulic load frame with an MTS model 634.31F-25 axial extensometer for strain-control tests while an Optris Laser thermometer monitored temperature generation.

Strain control fatigue specimens were in the form of cylindrical dog-bone shaped specimens as shown in Figure 9.

Figure 9   Cylindrical dog-bone shaped fatigue specimen geometry employed in this study of an Acrylonitrile Butadiene Styrene copolymer.

Fractography

Fracture surfaces of the fatigued specimens were obtained by first cutting the failed specimens using a Struers Minitom diamond cutter, and then coated using a Polaron 60/40 Au-Pl sputter coating system to allow SEM observation. Surfaces were first examined using an Axiovert optical microscope to obtain an overall fracture surface map. In addition, virgin specimens were cut from the as-received material and were ultrasonified for 15 minutes in a Branson 1510 to remove any impurities, followed by polishing on a Struers TegraPol-11 polishing machine, and SEM to determine the microporosity for the virgin ABS copolymer specimens. SEM was also used to determine the particle from which the initiated fatigue crack incubated for each specimen. An overall microscopy map which summarizes the optical and scanning electron microscopy observation process is depicted in Figure 10. Furthermore, energy-dispersive X-ray spectroscopy (EDS) was used to determine the composition of inclusions on the fracture surface and inclusions thought to be responsible for crack incubation.

Figure 10   An overall process map for optical imaging and scanning electron microscopy.

Furthermore, properties of particles responsible for incubation of fatigue cracks found on fracture surfaces are shown throughout this work are shown in Table 2.

Table 2 Incubating particle designations and properties for ten Acrylonitrile Butadiene
Styrene copolymer fatigue fracture surfaces.

Designation	Strain Amplitude	Frequency (Hz)	Equivalent diameter (μm)	Cycles to failure
S1	0.007	10	40.55	48679
S2	0.007	10	27.85	54479
S3	0.007	1	66.97	24170
S4	0.007	1	46.47	27786
S5	0.01	10	30.91	2986
S6	0.01	10	8.04	10375
S7	0.01	1	12.97	2767
S8	0.01	1	9.08	5123
S9	0.02	1	19.06	319
S10	0.04	1	18.42	160

CHAPTER III

MULTISTAGE FATIGUE (MSF) MODEL

Experimental and computational results were applied to an MSF model originally developed by McDowell *et al.* [2003] and used solely for metal alloys. The model focuses on three crack growth regimes summarized by Suresh *et al.* [2003]: incubation, microstructurally small crack (MSC) and physically small crack (PSC) growth, and long crack (LC) growth. The three regimes, which are based on fatigue damage formation and propagation, decomposes fatigue life as shown in Eq. (4-1).

$$_{otal} = Ni_{Inc} + Ni_{MSC} + Ni_{PSC} + Ni_{LC} = Ni_{Inc} + Ni_{MSC/PSCi} + Ni_{LC}. \tag{4-1}$$

Incubation

The equations for the incubation regime are designated as follows:

$$C_{inci} \ _{inc}^{\alpha} = \beta \tag{4-2}$$

$$\beta = \frac{\Delta \gamma_{max}^{p*}}{2} = Y[\varepsilon_a - \varepsilon_h]^q, \quad \frac{li}{Di} < \eta_{lim} \tag{4-3}$$

$$\beta = \frac{\Delta \gamma_{max}^{p*}}{2i} = Y(1 + \zeta z \ [\varepsilon_a - \varepsilon_h]^q, \quad \frac{l}{D} > \eta_{limi} \tag{4-4}$$

$$\frac{li}{Di} = \eta_{limi} \frac{\langle \varepsilon_a - \varepsilon_{th} \rangle}{\varepsilon_{per} - \varepsilon_{thi}}, \quad \frac{l}{Di} \leq \eta_{lim} \tag{4-5}$$

$$\frac{li}{Di} = 1 - (1 \mp \eta_{limi} \left(\frac{\varepsilon_{peri}}{\varepsilon_a} \right)^{ri}, \quad \frac{l}{Di} > \eta_{lim} \tag{4-6}$$

where,

$C_{\mathrm{inc}i}$	Linear coefficient in the modified Coffin-Manson law for incubation
	exponential coefficient in the modified Coffin-Manson law for incubation
N_{inc}	Number of cycles for incubation life
β	nonlocal damage parameter around an inclusion
$\frac{\Delta\gamma_{max}p^*}{2i}$	local average maximum plastic shear strain amplitude
ε_{ai}	remote applied strain amplitude
ε_{hi}	strain threshold for damage incubation
ε_{peri}	percolation limit for microplasticity
q	material related exponent from micromechanics simulations
	localization multiplier for β, based on FEA results as $l/D \rightarrow 1$
z	localization multiplier, where $z = (1/0.7) <l/D - 0.3>$
D	size of pertinent inclusion at which fatigue crack incubates
l	nominal linear dimension of the plastic zone size in front of the inclusion
$\frac{li}{Di}$	square root of the ratio of the plastic zone area over the inclusion area
η_{limi}	limiting ratio indicates the transition from proportional (constrained) micronotch root plasticity to nonlinear (unconstrained) micronotch root plasticity with respect to the applied strain amplitude
Y	parameter defined by $Y = y_1 + (1+R) y_2$, where y_1 and y_2 are model constants and R is the load ratio
r	shape constant for the transition to limit plasticity

Small Crack

The equations for the MSC regime are designated as follows:

$$\left(\frac{da}{dN}\right)_{MSCi} = \chi(\Delta CTDi - i\Delta CTDi_{hi}, \quad ai = i0.625D \tag{4-7}$$

$$\Delta CTD = C_{II}\left(\frac{GS}{GS_0}\right)_i^{\omega i}\left(\frac{GOi}{GO_0}\right)_i^{\xi}\left[\frac{U\Delta\hat{\sigma}i}{S_{uti}}\right]_i^{ni} ai + C_I\left(\frac{GS}{GS_0}\right)_i^{\omega i}\left(\frac{GOi}{GO_0}\right)_i^{\xi}\left(\frac{\Delta\gamma_{max}^P}{2i}\right)_i^{2i}i.i \tag{4-8}$$

where, i

$\left(\frac{da}{dN}\right)_{MSCi}i$ crack growth rate for MSC regime i

           material constant for a microstructure

a $\ddot{u}$ initial crack size contribution as a function of particle size

$\Delta CTD, \Delta CTDi_{hi}$ crack tip displacement range and threshold

C_I and C_{IIi} material dependent parameters for microstructural effects of MSC growth

GS, GS0   grain size and reference grain size

GO, GO$_0$ grain orientation and reference grain orientation

ω, ω'   exponents related to porosity effect on decreasing fatigue life

ξ, ξ'   exponents related to texture effects

n   exponent in small crack growth for low and high cycle fatigue respectively

$\Delta\hat{\sigma}i$ equivalent applied stress range

S$_{ut}$ ultimate stress

i

More exhaustive explanations on the MSF modeling equations can be found in literature [McDowell *et al.*, 2003; Xue *et al.*, 2007a; Xue *et al.*, 2007b; Xue *et al.*, 2007c; Xue *et al.*, 2007d; Xue *et al.*, 2010; Jordon *et al.*, 2010; Gibson, 2010]. i

CHAPTER IV

RESULTS AND DISCUSSION

Monotonic Loading

The effect of strain rate on the mechanical behavior of the ABS copolymer in tension and compression is presented in Figure 11, which shows the true stress–true strain response in an ambient laboratory environment at 25° C over a range of engineering strain rates (0.001/s, 0.01/s and 0.1/s). Average curves for test data were plotted with their respective error bars for all strain and temperature dependence plots. The stress response in tension shows the typical increase in the yield and peak stresses and a general flattening of the subsequent softening as strain rate increases which can be attributed to necking. The stress response in compression exhibits three regimes as noted in Figure 12b for compression temperature dependence: an initial linear elastic response followed by a non-linear transition curve to global yield, followed by strain softening attributed to chain rearrangement and subsequent strain hardening attributed to the alignment of these chains. An increased yield peak value with increasing applied strain rate was also observed, a behavior observed by Mulliken *et al.* [2005, 2006]; however, once the engineering strain rate reached 0.1/s for the ABS copolymer, a decrease in the subsequent strain hardening phase of deformation which is considered attributed to thermal softening in studies with another thermoplastic polymer [Arruda *et al.*, 1995].
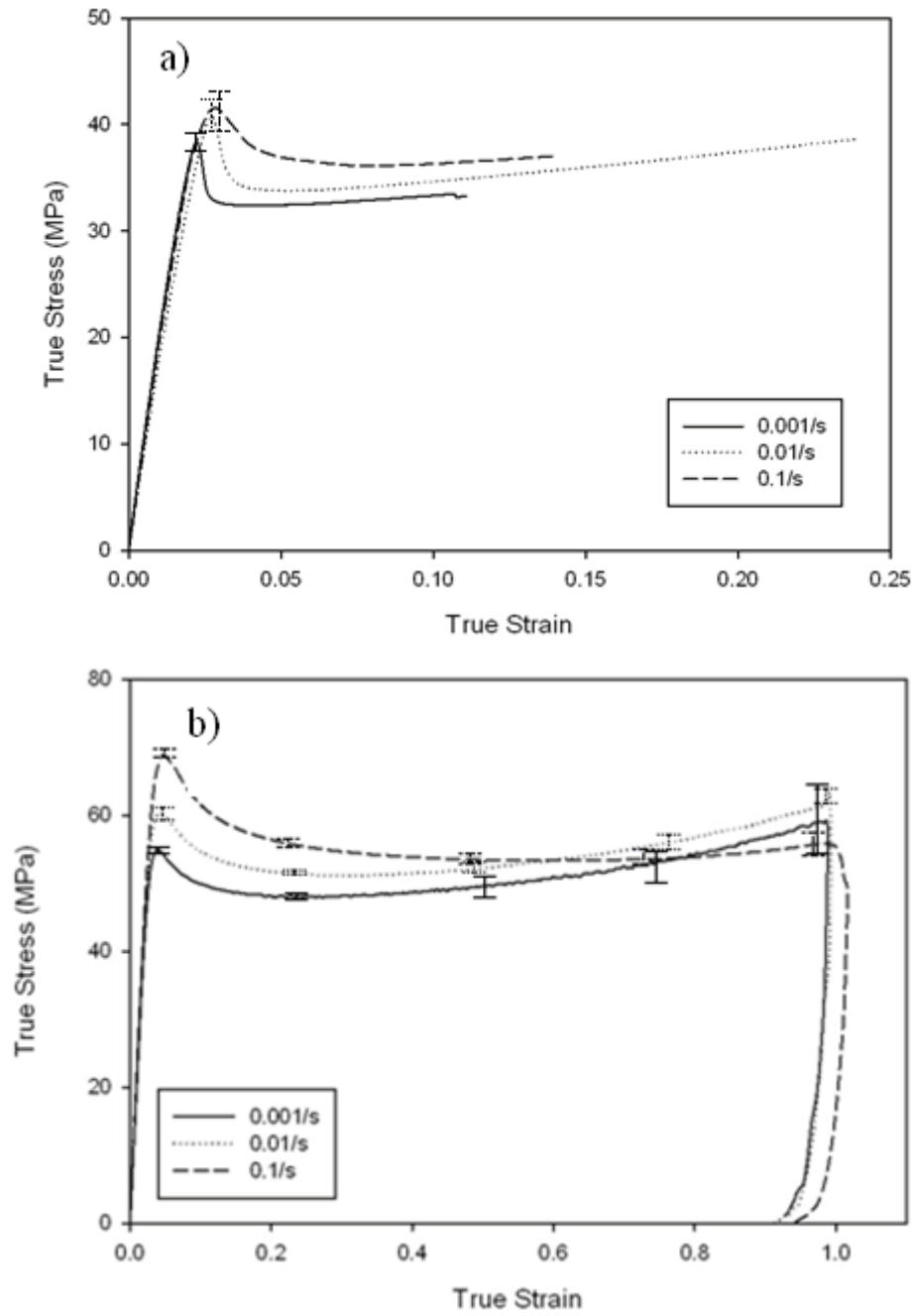
Figure 11 Monotonic strain rate dependence plots of an Acrylonitrile Butadiene Styrene copolymer in (a) tension and (b) compression.

Figure 12 shows the true stress–true strain response of ABS at 0.01/s in tension and compression respectively for different temperatures (-20° C, 25° C, 50° C, and 110° C). The initial Young's Modulus, yield stress, and hardening levels decrease as the temperature increased as shown by Richeton *et al.* [2006]. The residual strain after unloading decreases with increasing temperature; hence, the recovery effect of ABS seems to increase as temperature increases. For temperatures above the glass transition temperature, ABS is in a rubbery regime and a vanishing of the yield peak, strain softening and strain hardening is observed.
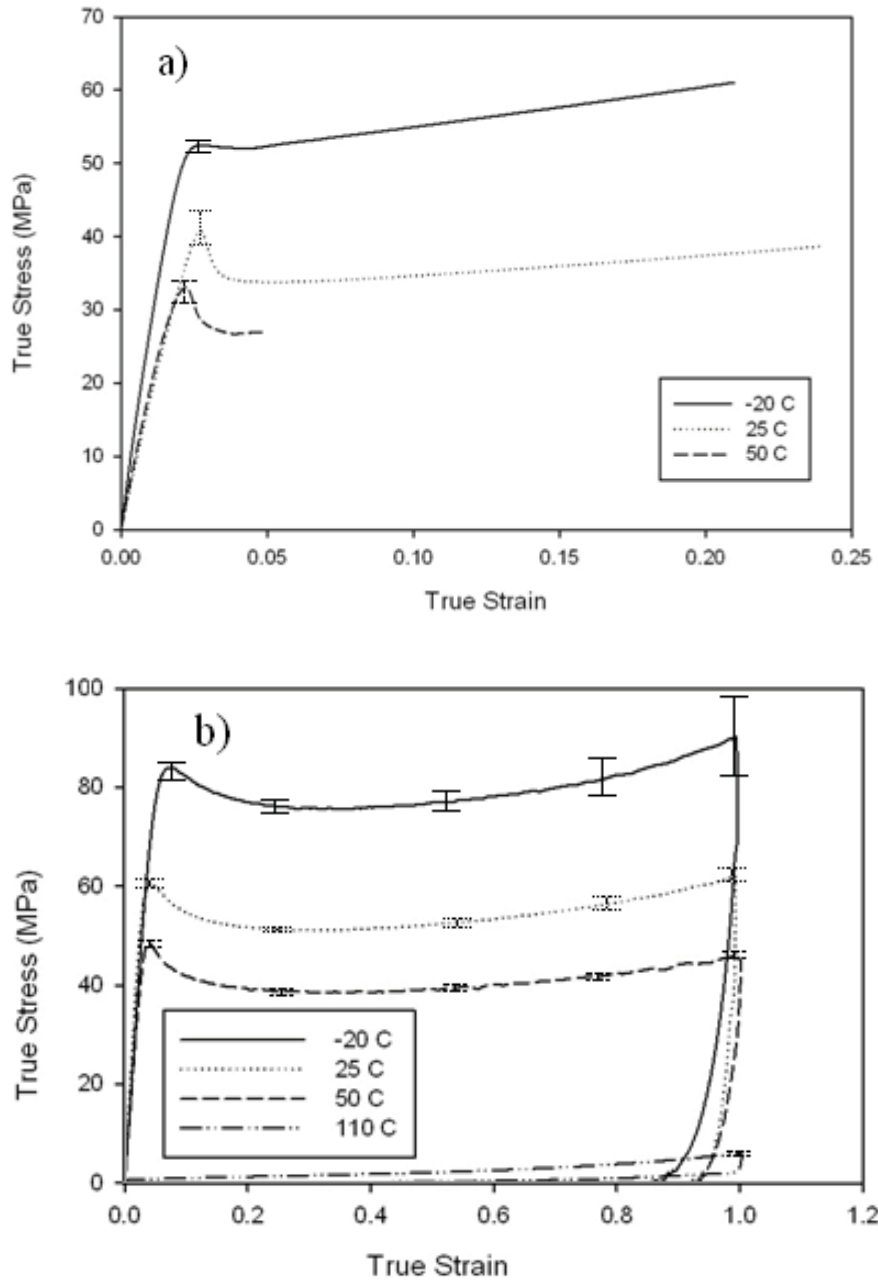
Figure 12   Temperature dependence plots for an Acrylonitrile Butadiene Styrene
copolymer tested at 0.01/s in (a) tension and (b) compression.

Microstructure

Image analysis software was used to quantify microstructural features for optical micrographs of the virgin ABS copolymer microstructure as shown in Figure 13. A minimum particle area of 1 μm^2 was used for a threshold analysis of the virgin material surface. Results from image analyses of the virgin microstructure are shown in Table 3. In addition, scanning electron micrographs of the porosity are shown in Figure 14.
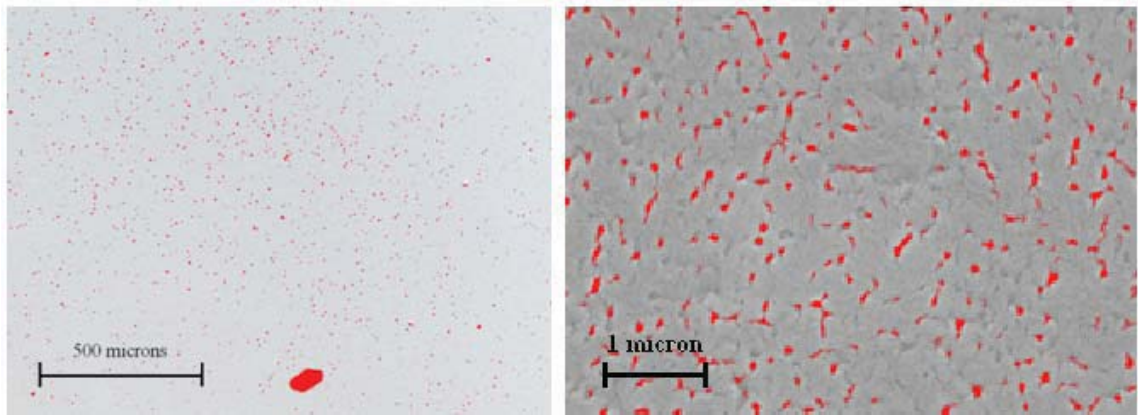
Figure 13   Optical micrographs of particles (left) and pores (right) of the virgin
microstructure of an Acrylonitrile Butadiene Styrene copolymer with a
minimum area of 1 μm^2.

Table 3   Particle and porosity properties obtained through image analysis of the virgin
microstructure of an Acrylonitrile Butadiene Styrene copolymer.

Average particle diameter (μm)	Average Nearest Neighbor (μm)	Standard Deviation (μm)	Minimum diameter (μm)	Maximum diameter (μm)
3.55	1.37	19.04	2.06	81.70

Average Pore Size (μm)	Pore Nearest Neighbor (μm)	Porosity (%)		
0.059	0.186	3.62		
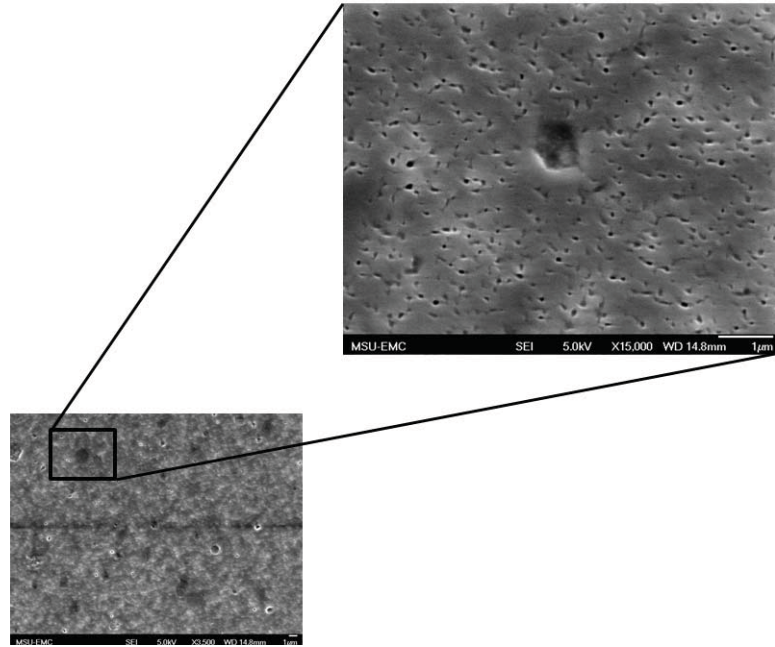
Figure 14   Porosity of an Acrylonitrile Butadiene Styrene copolymer was observed using scanning electron microscopy (scale bars are 1 μm).

A bin distribution of the particle sizes is shown in Figure 15. The majority of particles found on the virgin ABS microstructure are approximately 6 mm and smaller in equivalent diameter; however, the average particle size observed for initiating fatigue cracks on fracture surfaces of failed specimens was 28.77 μm, where; 8.04 μm < initiating particle size < 66.99 μm. Ten specimens (S1 through S10 from Table 2) are also shown in Figure 15.
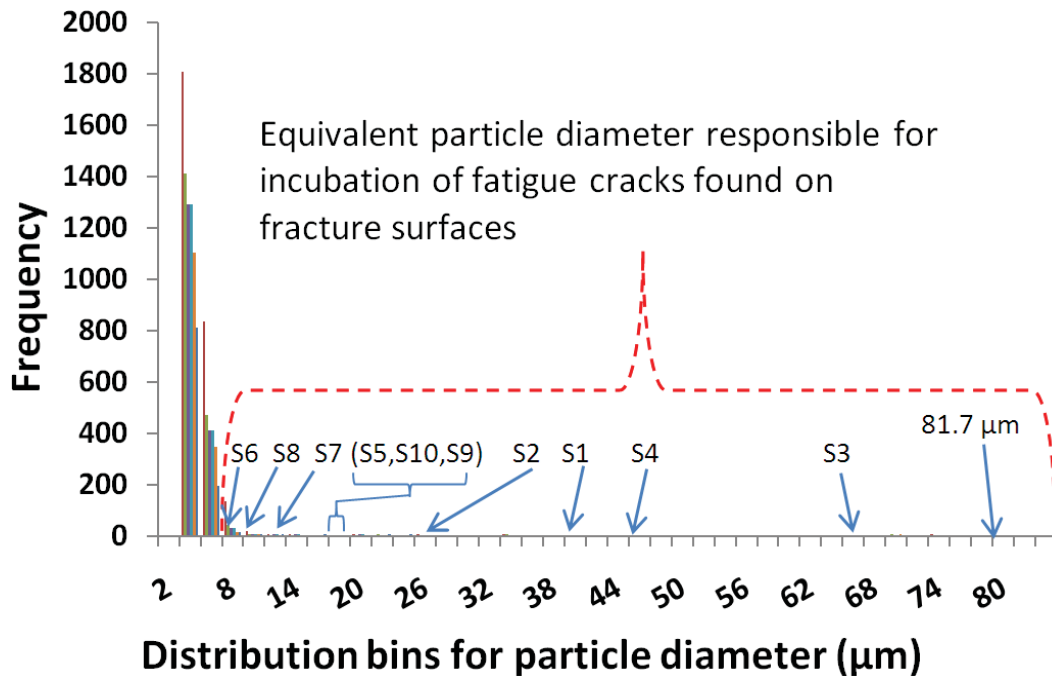
Figure 15   Equivalent particle diameter distribution on polished virgin surfaces for an Acrylonitrile Butadiene Styrene copolymer via optical microscopy with a minimum observed particle area of 1 μm^2 with S1 through S10 incubating particle designations.

Observations show defects responsible for incubating fatigue cracks are larger than the average particle sizes contained within the microstructure and follows work on MG alloys [Laz *et al.*, 1998; Gibson, 2010].

Marissen *et al.* [2001] observed that ABS was sensitive to defects with an approximate size of 20 μm, which is similar to the average defect size found responsible for incubating fatigue cracks in this work. Figure 16 shows a comparison of a particle from the fracture surface of an ABS specimen in this study, fatigued at 0.01 strain amplitude at 10 Hz, to a large defect found in an a fatigue study of ABS [Marissen *et al.*, 2001].
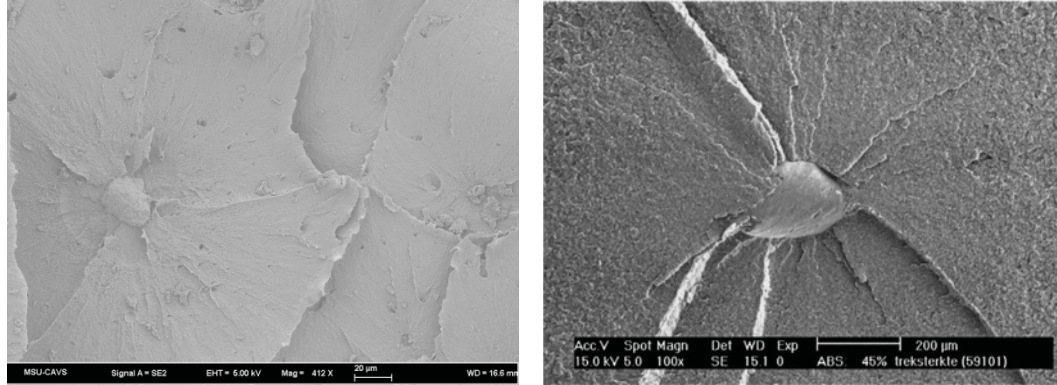
Figure 16 Comparison of particles found on fracture surface of: (a) particle found on Acrylonitrile Butadiene Styrene copolymer fatigue specimen used in this study (0.01 strain amplitude at 10 Hz) and (b) large defect found in work on ABS by Marissen *et al.* [2001].

Although there is a good correlation of average particle sizes found as defects within the ABS materials in this study compared to Marissen *et al.* [2001], different procedures for fatigue of specimens are used in the two works. ABS specimens in work by Marissen *et al.* were fatigued to 40% of the anticipated life and subsequently pulled in tension to failure disregarding the three fatigue regimes of incubation, MSC, and LC investigated in this work. Also, they do not quantify particle sizes responsible for incubation of fatigue cracks, but rather looks at fractured or debonded particles for the entire fracture surface (primarily from final fracture regime). However, the study does verify the content of the defects using a Raman imaging technique to quantify the content of acrylonitrile, butadiene, and styrene for the defects. The defect shown in Figure 16b was found to be mainly comprised of polybutadiene. Furthermore, large concentric structures of approximately 100 μm in diameter were observed by Marissen *et al.* [2001] around most of the average size defects. These defects were primarily composed of an

29

outer composition of acrylonitrile and polybutadiene where the defects themselves were primarily composed of polybutadiene using a Raman imaging technique.

In this study, large inclusions ranging from around 60 μm to approximately 81 μm were found within the virgin ABS copolymer surface through optical microscopy as shown in Figure 17. EDS analyses of defects or inclusions for this particular ABS copolymer point towards a primary composition of polybutadiene due to the high percentage of carbon with trace amounts of nitrogen can be attributed to small amounts of acrylonitrile. These large inclusions are thought to have initiated fatigue cracks in the lower 0.007 strain amplitude tests at 1 Hz.
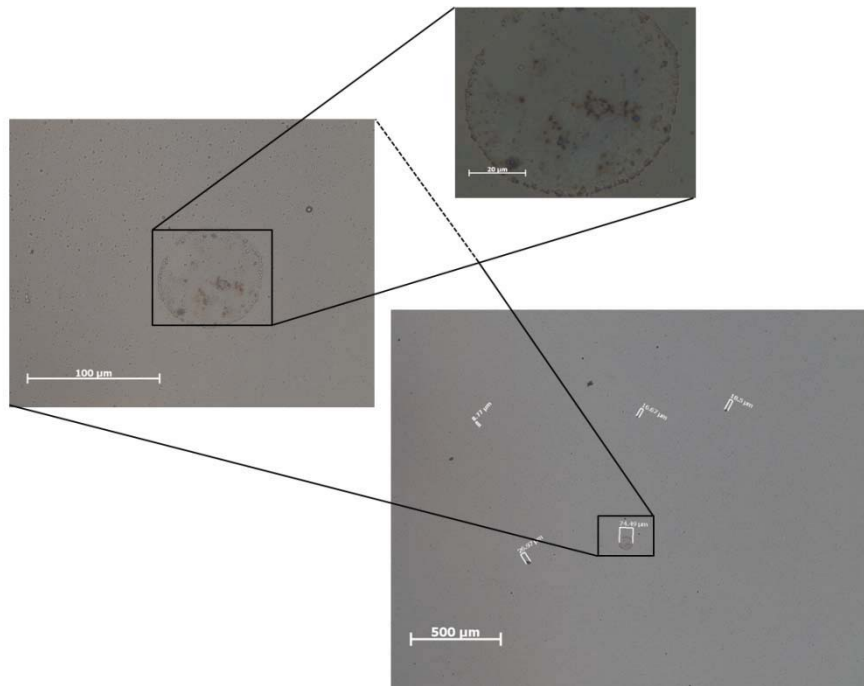
Figure 17   Axiovert optical micrograph showing distributed inclusions of varying sizes within the Acrylonitrile Styrene virgin material matrix and an exploded view of a large inclusion (approximately 74 μm).

The polybutadiene elastomer defects responsible for incubating fatigue cracks have a significantly lower modulus than the Acrylonitrile Styrene matrix. Cho [1999] showed the response of polybutadiene, even at a slightly higher engineering strain rate of 0.111/s compared to the 0.1/s for ABS in this work, exhibits a maximum true stress of about 0.19 MPa and an approximate strain to failure of 2.5 in tension. Typically, inclusions within the material matrix of materials for which the MSF model was applied have been stiffer than their respective matrices [McDowell *et al.*, 2003; Xue *et al.*, 2007a; Xue *et al.*, 2007b; Xue *et al.*, 2007d; Gibson, 2010]; however, this observation is inverted for the ABS copolymer. The work of Gall *et al.* (2000) examined different particle features from a micromechanical perspective, which was used to help develop the MSF model (McDowell *et al.*, 2003); in this work, Gall et al. (2000) assumed that the second phase could be a hard particle (harder and stiffer than the matrix) and a void (softer and less stiff than the matrix) and showed that the incubation regime of the model could act independently of the type of particle. Hence, although no engineering material has been examined via the MSF model in which the particle was softer than the matrix, clearly the original model would admit such a material.

Fatigue

Cyclic fatigue testing was performed on ABS copolymer specimens at 1 Hz and 10 Hz over a range of strain amplitudes (0.005, 0.0055, 0.0065, 0.007, 0.01, 0.015, 0.02, 0.025, 0.028, 0.03, 0.035, 0.04, and 0.05). A graph showing the strain-life data is shown in Figure 18, and an observation of longer lifetimes for higher frequencies is shown

following work by Marissen *et al.* [2001] and could partially be attributed to thermal softening for increased equivalent strain rates at 10 Hz [Arruda *et al.,* 1995].
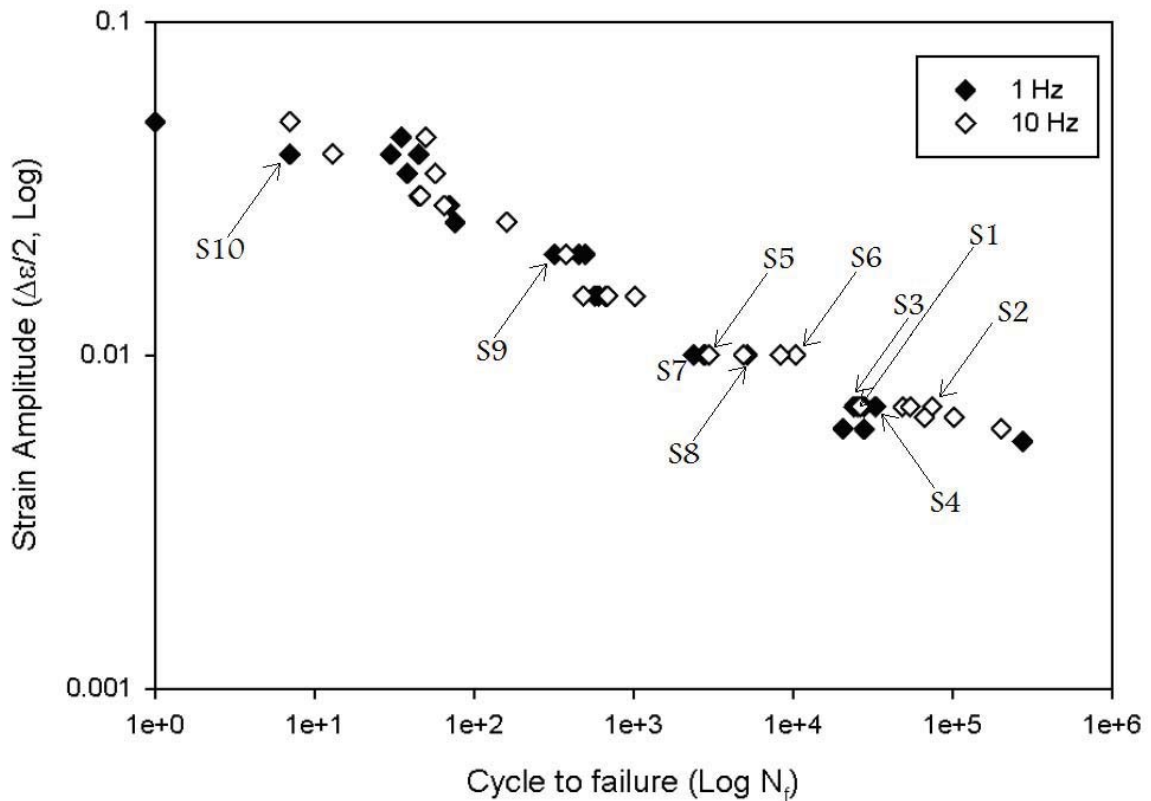
Figure 18 Acrylonitrile Butadiene Styrene strain control fatigue life plot for cylindrical dog bone fatigue specimens tested at 1 Hz and 10 Hz. Note: A run-out specimen was fatigued at 10 Hz at a strain amplitude of 0.005 for over 10 million cycles without failure.

Hysteresis and Stress Response

The first and half-life hysteresis loops for ABS specimens tested at 1 Hz and 10 Hz for increasing strain amplitudes (0.01, 0.02, 0.03, and 0.04) are shown in Figure 19.
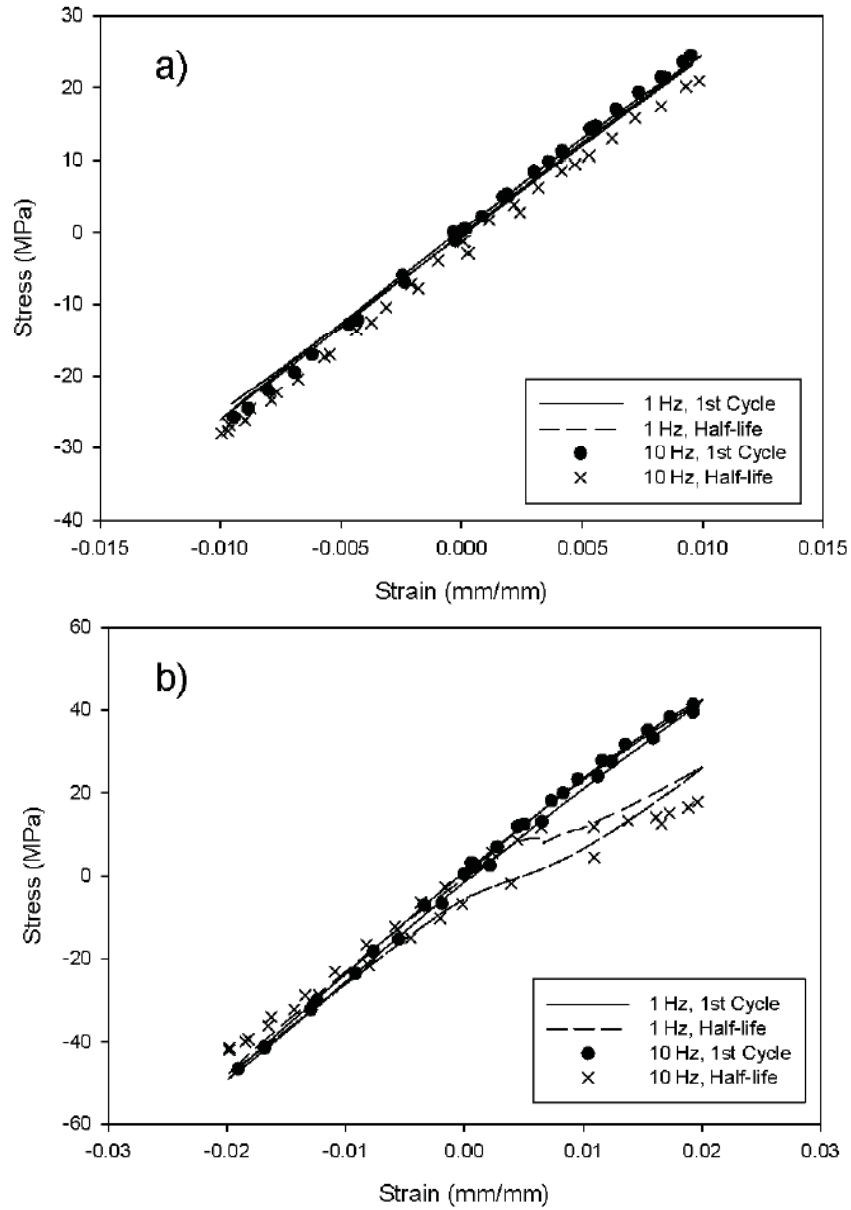
Figure 19 First cycle and half-life cycle hysteresis loops for an ABS copolymer tested at
1 Hz and 10 Hz with applied strain amplitudes of (a) 0.01, (b) 0.02, (c) 0.03,
and (d) 0.04.
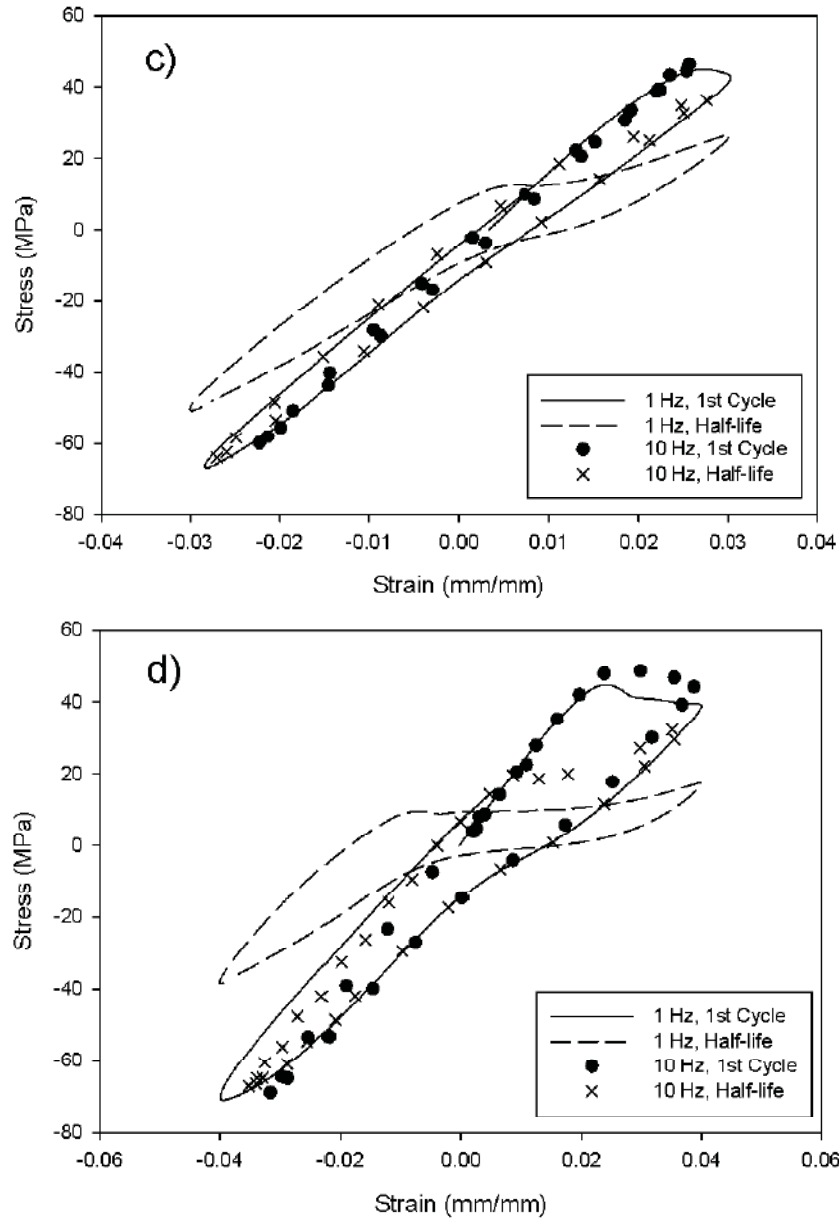
Figure 19 (continued)

For hysteresis loops of strain amplitudes of 0.01 and lower, a fairly linear behavior was observed for specimens fatigued at both 1 Hz and 10 Hz. As the strain amplitude reached 0.02, a reduction in stress in the tensile slopes for half-life cycles of specimens fatigued at 1 Hz and 10 Hz is observed. At 0.03 strain amplitude, a

broadening of the hysteresis loop begins to develop for specimens fatigued at both frequencies attributed to yielding of the ABS material. At 0.04 strain amplitude, a further broadening of the hysteresis loops is observed since the material is now beyond yield and in the deformation softening and hardening regime.

Figure 20 shows the peak tensile stress versus corresponding number of cycles to 50% load drop for ABS fatigue specimens tested at 1 Hz and 10 Hz, respectively. As strain amplitudes reach above 0.015 strain amplitude the reduction in tensile stress versus cycles becomes more apparent for both 1 Hz and 10 Hz specimens. The temperature generated could be considered negligible until 0.02 strain amplitude, where the decrease in stress versus fatigue life becomes more prevalent. At strain amplitudes of 0.02 and greater, a reversal in the fatigue life to 50% load drop was observed where 10 Hz specimens reach this drop sooner. This phenomenon could be attributed to the higher stresses induced through the equivalent higher strain rate at 10 Hz, leading to a more dominant thermal softening of the material.
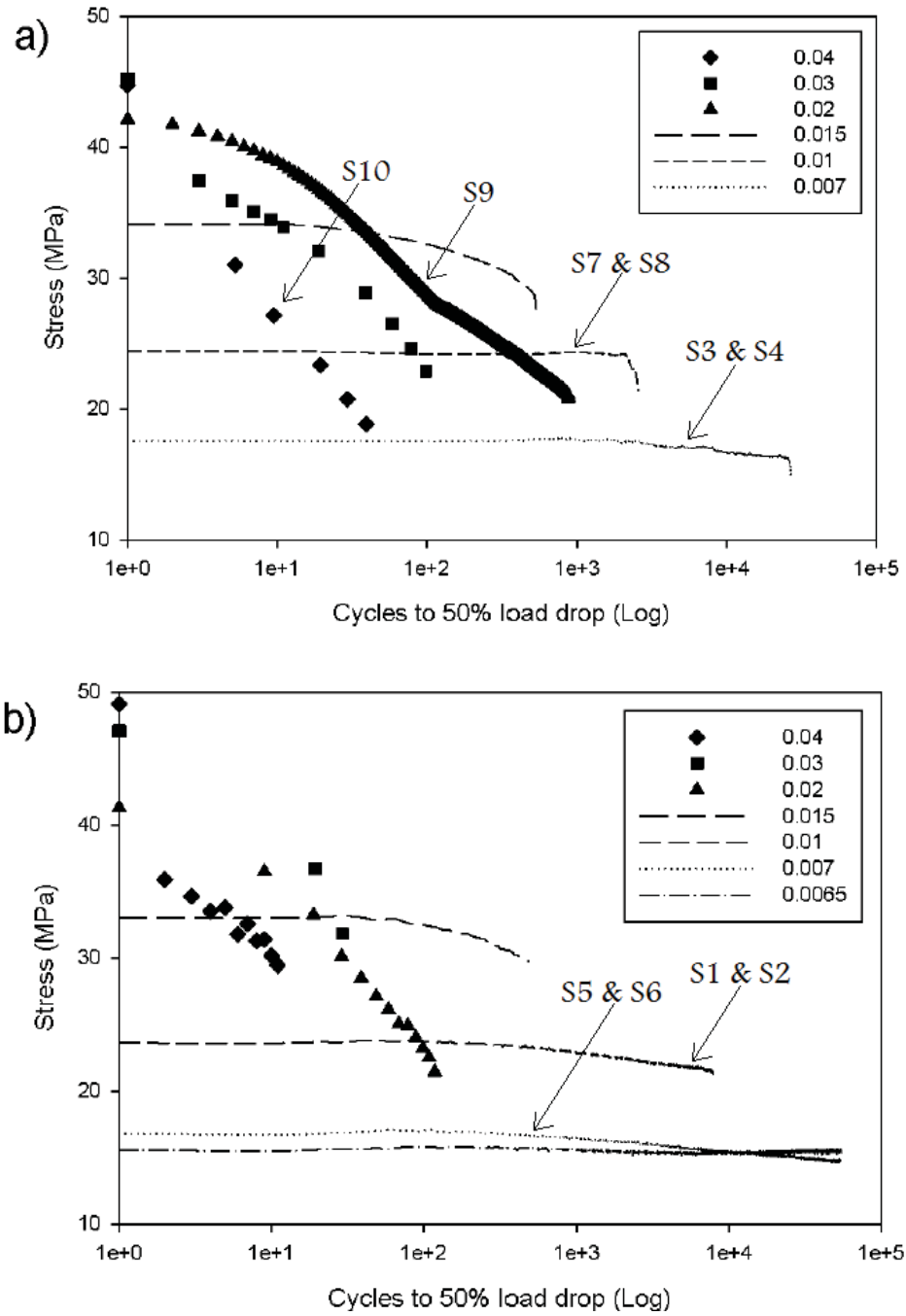
Figure 20 Peak tensile stress versus number of cycles to 50% load drop for increasing applied total strain amplitudes for ABS fatigue specimens performed at (a) 1 Hz and (b) 10 Hz.

Temperature Generation

The temperature of the specimen surface for strain control fatigue tests was monitored using an Optris laser thermometer for specimens fatigued at 1 Hz and 10 Hz over a range of strain amplitudes (0.007 to 0.05). The temperature generated at the surface for each fatigue specimen was plotted verses the corresponding strain amplitude as shown in Figure 21.
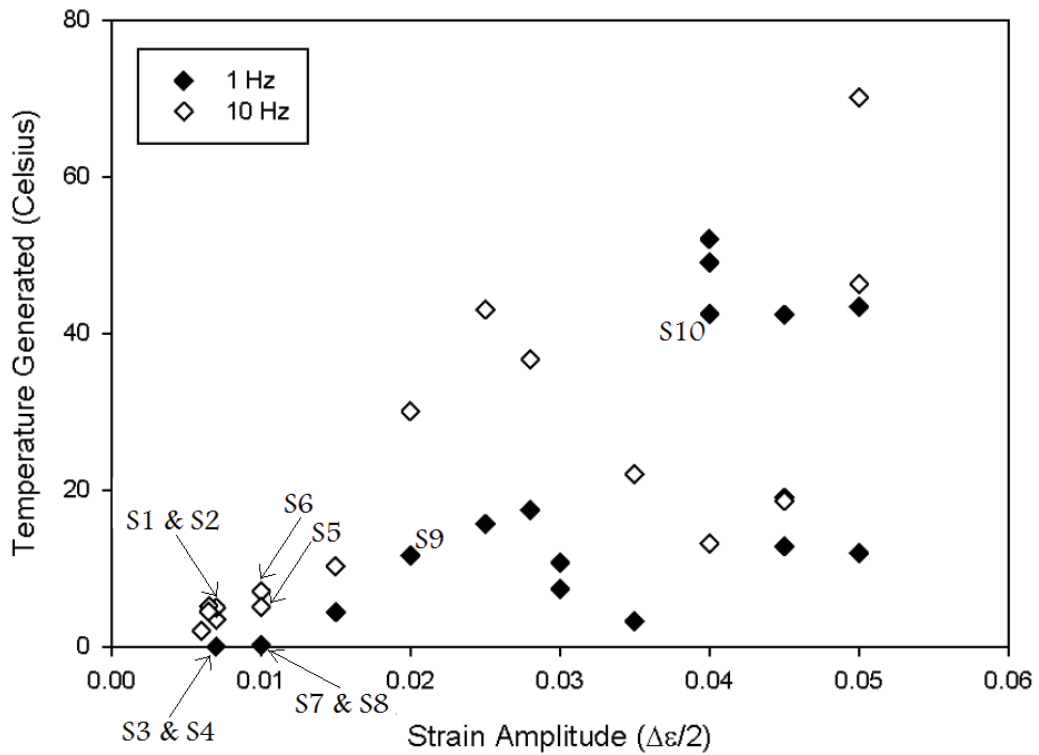
Figure 21   The temperature generation profile for initially ambient temperature
Acrylonitrile Butadiene Styrene copolymer fatigue specimens tested at 1 Hz
and 10 Hz at corresponding strain amplitudes.

An increase in the temperature generated at the specimen surface during fatigue tests was observed throughout the elastic regime to strains of approximately 0.025 for 1

Hz and 0.028 for 10 Hz which corresponds to yielding of the ABS copolymer. Beyond yield, the temperature generated began to decrease throughout the viscoplastic regime to 0.035 strain amplitude for 1 Hz and 0.04 strain amplitude for 10 Hz. The subsequent increase in temperature generated was observed throughout the deformation-induced hardening regime to failure.

The increase in temperature to yield could be attributed to the stretch and ordering of polymer chains. The polymer chains are aligned at yield and begin to stretch until ultimate failure [Felton, 2007]. The subsequent softening beyond yield and lower temperature generation could be attributed to the breaking or slipping of some of the shorter polymeric chains, necking, or also through craze formation. Furthermore, the final increase in temperature generated to failure could be attributed to the overall stretch, alignment, and final fracture of remaining long polymer chains. In general, the temperature generated was higher for ABS specimens fatigued at 10 Hz when compared to 1 Hz. An interesting observation at 0.04 strain amplitude shows 1 Hz specimens with a higher temperature generation when compared to 10 Hz specimens fatigued at the same strain amplitude. This could be attributed to the increase in equivalent engineering strain rates for the 10 Hz fatigue specimens, which broadens the global yield to a higher peak strain, and therefore leads to a higher realized strain prior to the temperature dwell observed beyond yield.

This phenomenon could be characterized as a texture effect for the ABS copolymer when observing the monotonic tensile data beyond yield and throughout necking. The evolving texture effect was not captured by the current MSF model for the ABS copolymer and this study; however, the MSF model is capable of capturing solid-

state texture effects for metal alloys through attributes such as grain size and orientation. The ability to capture evolving texture effects, especially for polymers due to their higher sensitivity in processing and loading in general, should be developed for the MSF model in future work.

Fractography

Fractography was performed on the fatigue fracture surfaces of the fatigue ABS copolymer specimens using scanning electron microscopy (SEM) to characterize the fatigue regimes: incubation, microstructurally small crack (MSC), and long crack (LC) growth and also quantify sizes of particles from which fatigue cracks incubated. An overall fracture surface map for ABS fatigue specimens fatigued at a range of strain amplitudes (0.007, 0.01, 0.015, and 0.02) and frequencies (1 Hz and 10 Hz) are shown in Figure 22. SEM analysis of fracture surfaces showed that debonded or fractured particles near the free surface had incubated fatigue cracks for the ABS copolymer specimens.
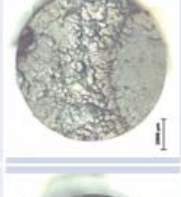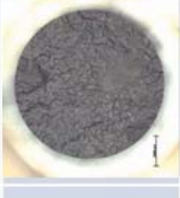
	$\varepsilon_A = 0.02$		$\varepsilon_A = 0.015$		$\varepsilon_A = 0.01$		$\varepsilon_A = 0.007$	
$\omega = 1$ Hz	S9				S7	S8	S3	S4
	$N_f = 319$	$N_f = 495$	$N_f = 483$	$N_f = 670$	$N_f = 2{,}767$	$N_f = 5{,}123$	$N_f = 24{,}170$	$N_f = 27{,}786$
$\omega = 10$ Hz					S5	S6	S1	S2
			$N_f = 688$	$N_f = 1{,}024$	$N_f = 2{,}986$	$N_f = 10{,}375$	$N_f = 48{,}679$	$N_f = 54{,}479$

Figure 22 Overall fracture surface map for ABS strain-control fatigue specimens showing a general trend of smoother fracture surfaces as strain amplitude was decreased and a rougher fracture surface containing facets similar to those seen in studies by Marissen *et al.* [2001] as strain amplitude was increased.

A comparison of fracture surfaces for specimens performed at 0.007 and 0.01 strain amplitudes at both 1 Hz and 10 Hz respectively, are shown in Figure 23. As the strain amplitude is decreased, the fracture surface becomes smoother due to lower crack growth rates. At higher frequencies, there is a higher equivalent strain rate observed and a slower crack growth rate also leading to a smoother fracture surface which follows observations by Ishikawa and Ogawa [1981] for glassy polymers.

(A) S3

(B) S8
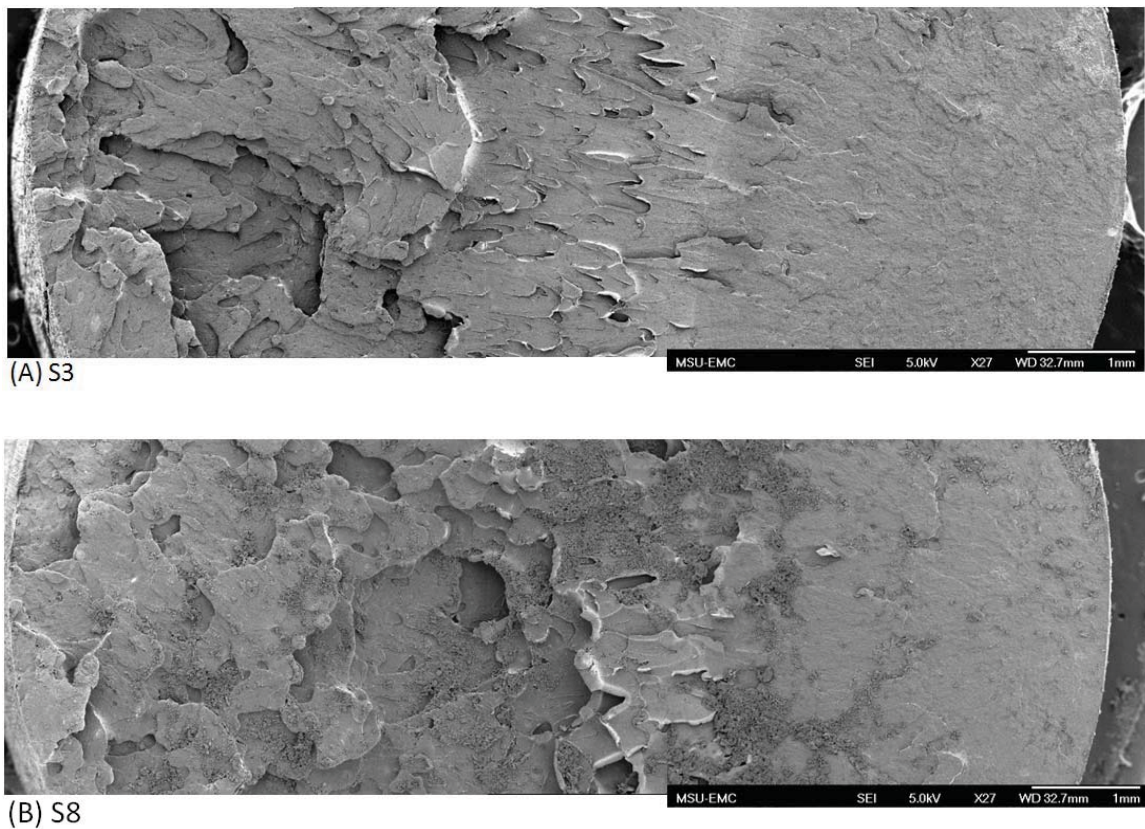
Figure 23   Fracture surface maps of Acrylonitrile Butadiene Styrene copolymer fatigue specimens designating the different regimes of crack growth for frequencies and strain amplitudes of: (a) 1 Hz, 0.007, (b) 1 Hz, 0.01, (c) 10 Hz, 0.007, and (d) 10 Hz, 0.01.
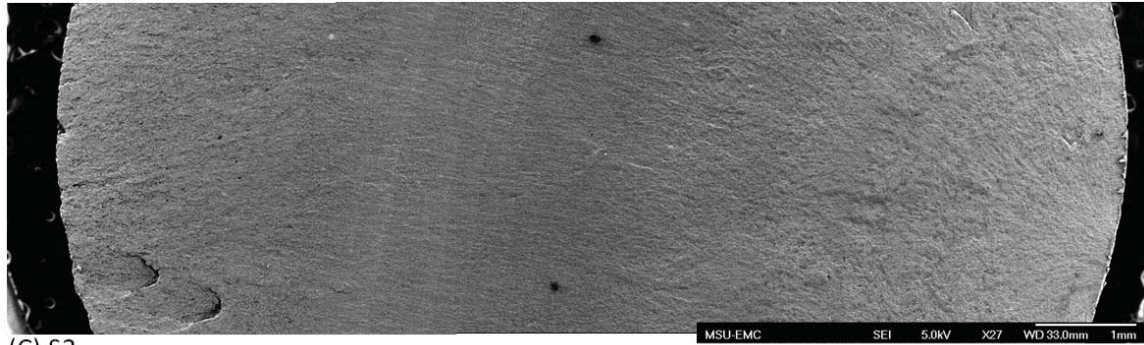
(C) S2
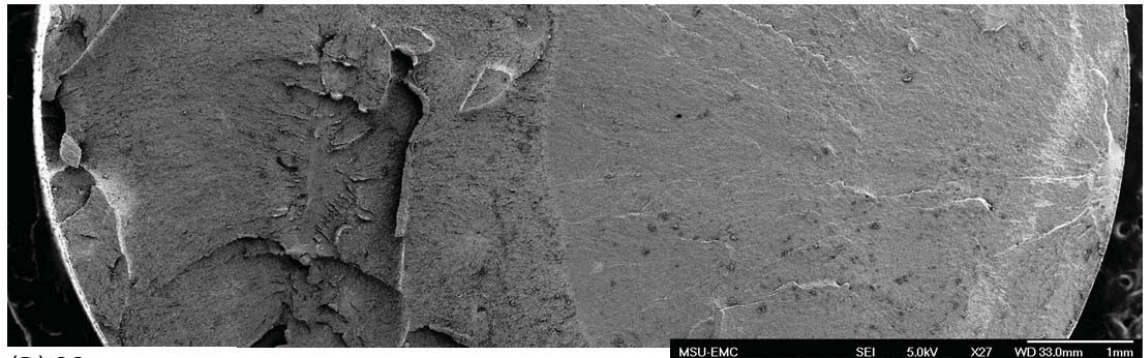
(D) S6

Figure 23 (continued)

Simple observations of the fracture surface will not yield percentages for the three fatigue regimes; however, incubation can be estimated at 15% for the ABS copolymer due to the typical defect sizes responsible for incubating fatigue cracks and the nano-porosity contained within the material matrix [McEvily *et al.*, 1963; Radon, 1979; Maiti *et al.*, 2005; Xue *et al.*, 2007d; Weiland *et al.*, 2009].

Furthermore, scanning electron microscopy was used to quantify the square root of the particle areas for particles from which fatigue cracks incubated for respective upper and lower bounds of fatigue life. The respective square root particle areas and number of cycles to failure are also shown for each specimen in Figure 24.

S1
$N_f = 48,679$ $D = 40.55$ µm

S2
$N_f = 54,479$ $D = 27.85$ µm

(a)

S3
$N_f = 24,170$ $D = 66.97$ µm

S4
$N_f = 27,786$ $D = 46.47$ µm

(b)

S5
$N_f = 2,986$ $D = 30.91$ µm

S6
$N_f = 10,375$ $D = 8.04$ µm

(c)

S7
$N_f = 2,767$ $D = 12.97$ µm

S8
$N_f = 5,123$ $D = 9.08$ µm

(d)

S9
$N_f = 319$ $D = 19.06$ µm

S10
$N_f = 35$ $D = 18.42$ µm

(e)
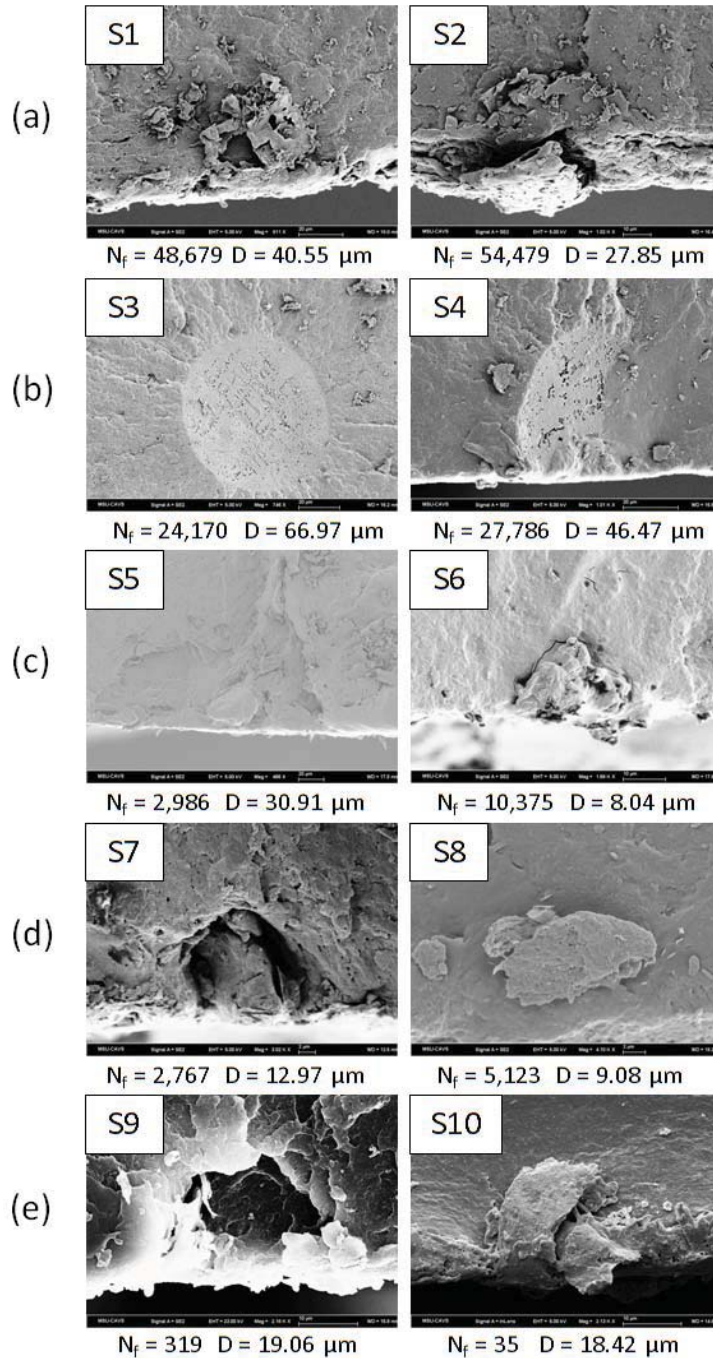
Figure 24   Scanning electron micrographs for particles responsible for incubating fatigue cracks for upper and lower bounds of fatigue life of Acrylonitrile Butadiene Styrene copolymer specimens where N_f is the number of cycles to failure and D is the square root particle area.

43

Figure 25 shows the methodology for finding the initiating particle using scanning electron microscopy.
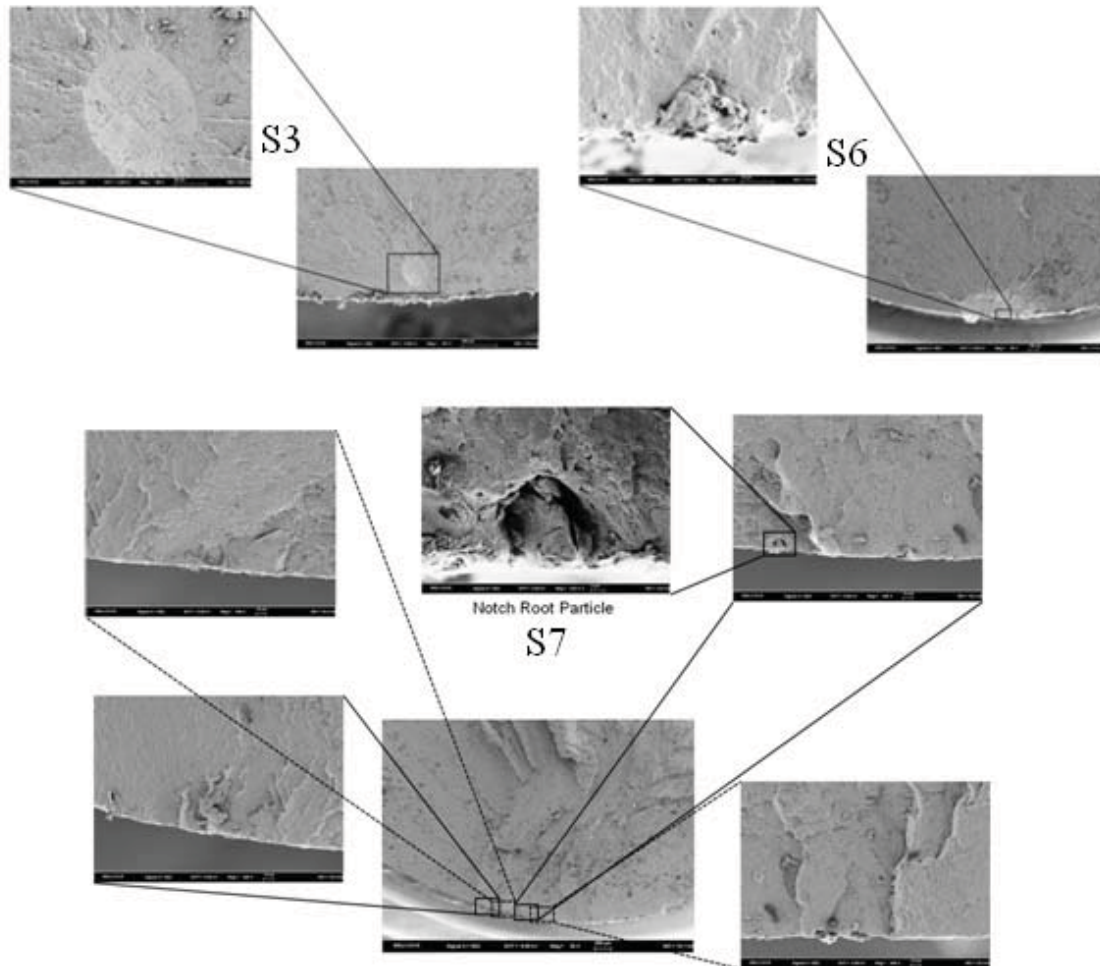
Figure 25   Scanning electron microscopy was used to locate the initiating particle sizes from which fatigue cracks incubated for the Acrylonitrile Butadiene Styrene copolymer specimens S3, S6 and S7.

Large inclusions with an approximate square root area between 46.47 μm and 66.97 μm, and fractured particles near the free surface ranging from 8.04 μm to 40.55 μm in equivalent square root area, were found to be the initiation sites on most ABS

44

copolymer fracture surfaces. The larger inclusions found within the virgin matrix, previously shown in Figure 17, are comparable in size and shape to the inclusions in which fatigue cracks incubated for specimens fatigued at 0.007 strain amplitude at 1 Hz as shown in Figure 24 (specimens S3 and S4).

Figure 26 shows particle sizes responsible for incubating fatigue cracks found from ABS specimen fracture surfaces versus cycles to failure. A trend was observed where larger particles from which fatigue cracks incubated for a given strain amplitude and frequency failed at a lower number of cycles. The negative slope further supports observations of larger particles leading to lower fatigue lifetimes and a similar trend is shown in works with metal alloys [Bernard, 2010; Gibson, 2010].
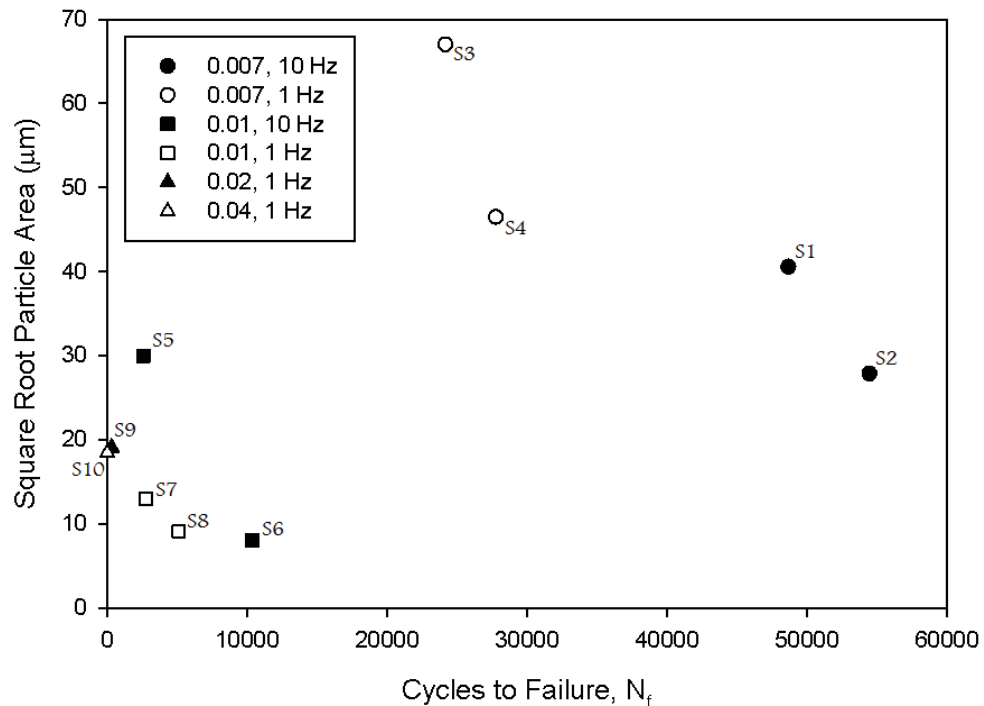
Figure 26 Square root particle size area responsible for incubation of fatigue cracks for respective strain amplitudes and frequencies for an Acrylonitrile Butadiene Styrene copolymer versus cycles to failure.

A cartoon depiction of particles sizes on a strain-life fatigue plot is shown in Figure 27. The visual representation where larger particles yielding lower fatigue lifetimes is shown where strain effects are shown to be more prevalent for the lower strain amplitude where larger defects were prone to initiate fatigue cracks.
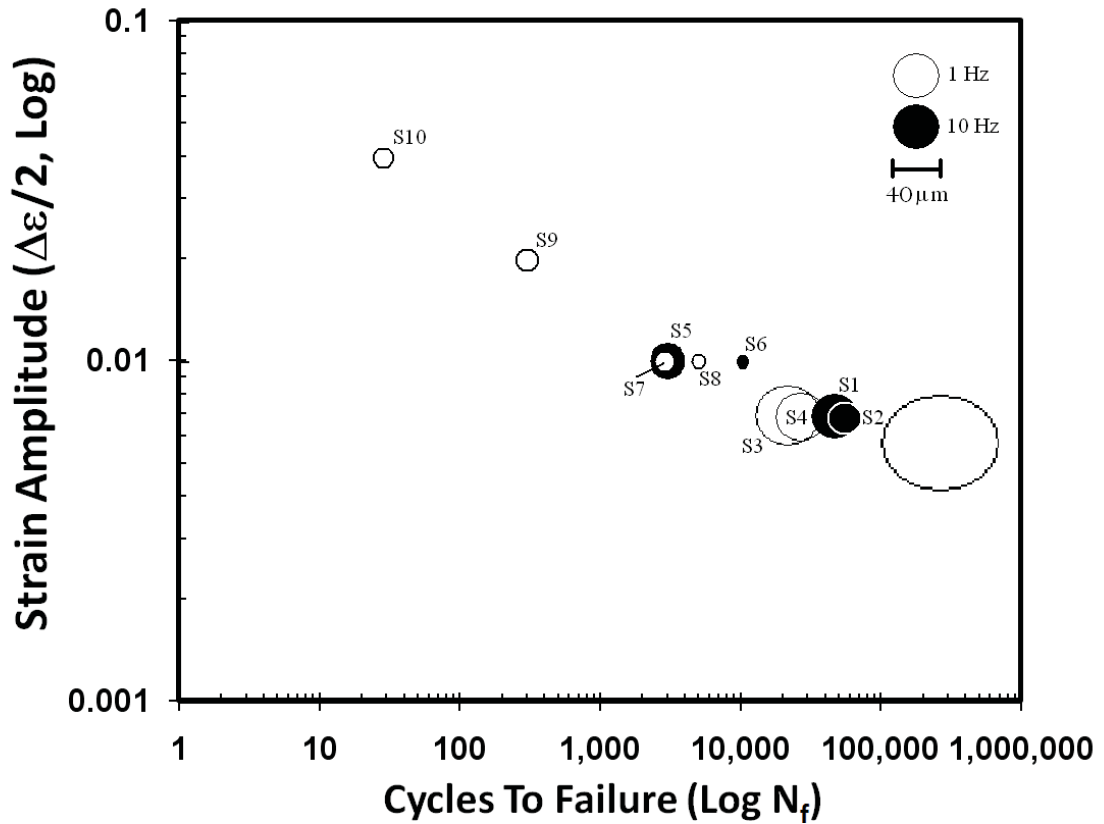
Figure 27 Log-log plot of strain amplitude versus cycles to failure for an Acrylonitrile Butadiene Styrene copolymer showing high cycle fatigue is more sensitive to large defects and equivalent strain rates for 1 Hz and 10 Hz.

Larger particles lead to lower fatigue lifetimes due to higher stress concentrations initiating fatigue cracks. In the low cycle fatigue regime for the ABS copolymer, where strain amplitude applied is greater than 0.01, fatigue life appears to be less sensitive to

particle size. This could be attributed to massive amounts of plasticity and deformation distributed throughout the material in the low cycle regime. In the high cycle regime, there appears to be more sensitivity to larger defects as well as frequency as the effect of time and stress concentration becomes more localized.

MSF Model Correlations

For the preliminary model for the ABS copolymer, the values for strain threshold and percolation, q, η_{lim} and r were set using previous micromechanics simulations by Xue *et al.* [2007d].

χ was determined for the ABS copolymer, where $\chi = \sigma_e/TS = 0.0698$ [McClintock *et al.,* 1999]. The crack tip displacement threshold, $\Delta CTD i_h$, which is generally assigned a value on the order of the Burger's vector for metal alloys, was taken as the magnitude of the shear displacement of the sheared region of an amorphous polymer [Bowden, 1974]. Values for C_I, C_{II}, α, and C_n were obtained using a best fit for the ABS copolymer. ***GS/GS$_0$, GO/GO$_0$, ξ, ξ', v***, and ***v'*** are material constants typically used to describe grain orientation and size effects within metal alloys [McDowell, 2003; Gibson, 2010]. These values were set to 1 in this study for the ABS copolymer; however, an evolving texture effect should be introduced in future work. ω, an exponent related to the porosity effect towards fatigue life was set to zero for simplicity and due to lack of experiments. n is related to the slope of the log-log plot for $\frac{da}{dNi}$ versus the stress ratio $\frac{\sigma_{ai}}{\sigma_{bi}}$, where σ_a is the strain amplitude and σ_b is the ultimate tensile stress [Shiozawa *et al.* 1997]. For the ABS copolymer, the exponent n was approximated following Xue *et al.*

[2007d] by using the slope of the da/dN versus ΔK from work performed by Kim *et al.* [1994].

The load path dependent and loading combination parameter, θ, used to find the equivalent applied stress range, and introduced by Hayhurst et al. [1985] to model combined stress state effects, was set to zero for this work due to lack of torsion fatigue experimental data; therefore, $\Delta\hat{\sigma}$ is equivalent to the range of maximum principal stress.

The long crack growth regime of the MSF model has historically followed classical linear elastic fracture mechanics approaches [Xue *et al.,* 2007d; Jordon *et al.*, 2010]; however, the modeling approach presented in this study is focused on incubation and MSC regimes of the ABS copolymer.

Maximum and minimum strain amplitudes applied in experiments, along with cycles to failure for corresponding strain amplitudes, when then included in the model. Image analyses of optical and scanning electron micrographs of polished virgin ABS specimens, as shown previously in Figures 13, 15 and 17, were performed to obtain particle and pore properties as shown in Table 2.

Next, monotonic stress strain behavior was compared to the cyclic stress-strain behavior as shown in Figure 28. The maximum tensile stress of stabilized hysteresis loops at respective strain amplitudes was plotted for the cyclic stress-strain curve to obtain the cyclic strength coefficient and hardening exponent for the ABS copolymer following Bannantine *et al.* [1990].
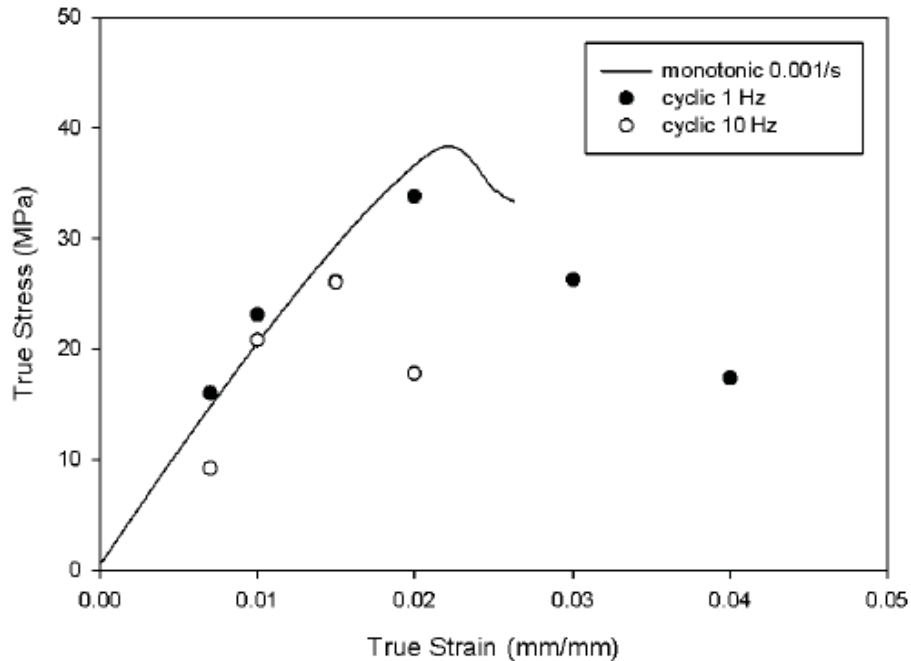
Figure 28 Monotonic tensile and cyclic stress versus strain behavior for fully reversed experiments at half lifetime for an Acrylonitrile Butadiene Styrene copolymer.

Incubation life was fit to approximately 15%, as shown in Figure 29, using the modified coffin manson law coefficient and exponent parameters. The maximum and minimum particle sizes observed on fatigue fracture surfaces and responsible for incubating fatigue cracks were employed in the MSF model to capture error bands for the ABS copolymer. Using the extreme values for particles observed on the ABS virgin material surface, a maximum particle size of 81.7 μm and a minimum of 2.06 μm were used to obtain the upper and lower bounds for the MSF model as shown in Figure 30. The particle sizes selected for the upper and lower bounds of the MSF model was based on the extreme particle sizes from optical micrographs analysis and represents the variation of the ABS copolymer microstructure.
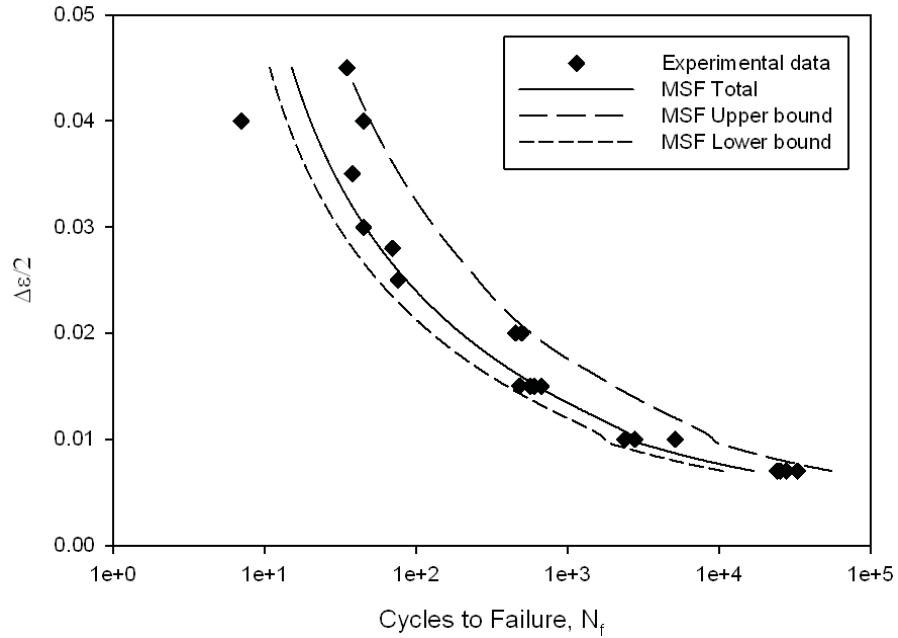
Figure 29 MSF incubation life plotted with experimental fatigue data and total life fit for the Acrylonitrile Butadiene Styrene copolymer.
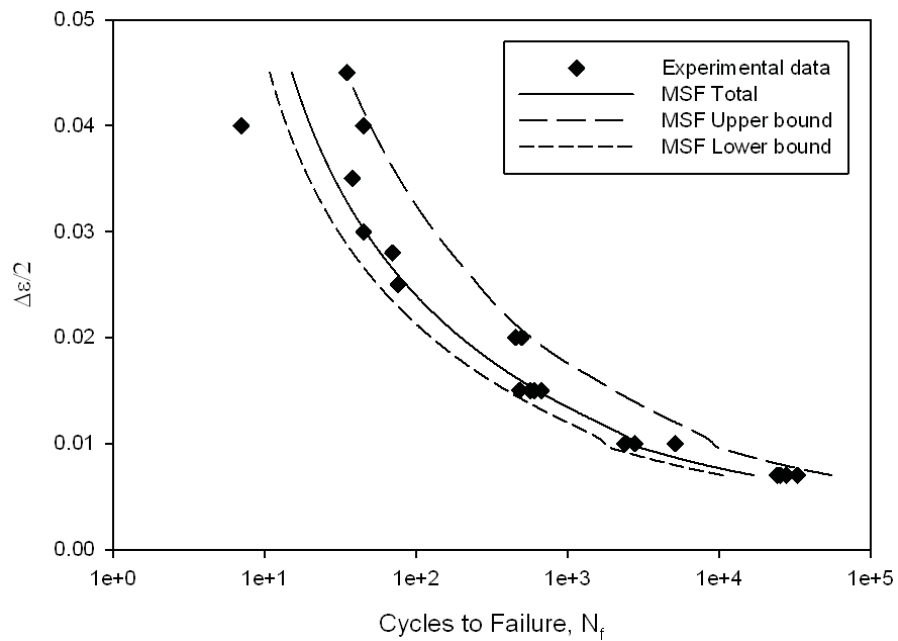
Figure 30 MSF total life correlation of experimental fatigue data shown with upper and lower bounds for the Acrylonitrile Butadiene Styrene copolymer.

Table 4 shows the model constants used to correlate the MSF to the experimental

fully reversed uniaxial strain life results for the ABS copolymer.

Table 4   MSF parameters and material properties for an Acrylonitrile Butadiene
Styrene.

Property	Value
n	2.55
α	-0.665
C_n	0.48
CTD_{thi}	$4.25 \times 10^{-4i} \mu m$
C_{Ii}	$1.6 \times 10^{4i} \mu m i$
C_{IIi}	$1.82 \ \mu m$
ri	0.1
C_{inci}	0.17
q	2.367
y_{1i}	100
y_{2i}	0

CHAPTER V

CONCLUSIONS

Cyclic fatigue behavior for a thermoplastic ABS copolymer was quantified with microstructural properties which govern uncertainty of the mechanical response. In addition, the MultiStage Fatigue (MSF) model was used to capture these microstructural features and effects on strain-life fatigue behavior. The following conclusions and recommendations were derived through this study.

- Monotonic compression tests reveal a reduction in stress at the second peak region at 0.1/s which follows observations by Arruda *et al.* [1994] for glassy polymers where the phenomenon is attributed to thermal softening of the polymeric material.

- Energy-dispersive X-Ray spectroscopy results show the defects responsible for incubation or initiation of fatigue cracks are primarily composed of carbon which can be attributed to polybutadiene. In addition, trace amounts of nitrogen on some defects shows some acrylonitrile is possibly present. Similar findings for the composition of defects in ABS copolymers using a Raman imaging technique was found in work by Marrisen *et al.* [2001].

- Although no engineering material like the ABS copolymer has been correlated to the MSF model where particle was softer than the matrix prior to this work, clearly the MSF model would admit such a material, based on studies by Gall *et al.* [2000].

- Fatigue cracks for the 0.01 strain amplitude and lower tests were found to initiate at particles on or near the free surface of the cylindrical fatigue specimens. Fracture surfaces for strain amplitudes of 0.015 to 0.02 show a similar distributed faceting on fracture surfaces as seen in studies performed by Marissen *et al.* [2001]. Fatigue specimens performed at 0.025 to 0.035 strain amplitude show quick decreases in peak tensile stress versus number of cycles and the fracture surfaces are difficult to observe due to massive thermo-mechanical degradation. Fracture surfaces of 0.04 strain amplitude specimens are similar to those performed at 0.01 strain and lower as they are glossy in texture and show no signs of faceting.

- A negative slope of particle size responsible for incubation of fatigue cracks versus the number of cycles to failure follows similar work on metal alloys [Bernard, 2010; Gibson, 2010] and shows that failure mechanisms such as debonded particles have similar effect on the fatigue lifetime independent of the material observed.

- Tests performed at higher frequencies led to higher fatigue lifetimes which could be attributed to the thermal softening of the polymer which relieves stress rather than degradation through other failure mechanisms such as crazing or shear banding.

- Degradation of inclusions in the form of cavitation due to mechanical and thermal loading, as well as volume expansion should be considered for future micromechanical simulations for the ABS copolymer and other similar filled polymers. In addition, further investigation into degradation mechanisms including crazing and shear banding need to be performed for possible inclusion in MSF modeling of polymers as possible texture effects. Texture effects for polymers were not introduced in this work and future work and extension of the MSF should include

an "evolving" texture effect for polymers. Furthermore, studies on the competing influence of frequency and temperature effect due to environmental subjection or generation is needed, as the current MSF model does not capture these effects.

- This work was a preliminary introduction of an ABS copolymer to the MSF model. For this preliminary model for ABS, the MSF model was able to account for differences in defect sizes to capture the fatigue behavior of a thermoplastic ABS copolymer. Note that the parameters found through micromechanics simulations by McDowell *et al.* [2003] and Xue *et al.* [2007d] were used in this study, and some parameters need to be found for the ABS copolymer through micromechanics simulations and crack growth experiments. Ultimately, by simply utilizing the maximum and minimum particle sizes which incubated fatigue cracks, the MSF model was able to capture the upper and lower bounds of fatigue on the strain-life curve. This observation illustrates the capability of the MSF model to capture the microstructural effects on the fatigue properties of polymeric materials.

REFERENCES

Adams ME, Buckley DJ, Colborn RE, England WP, Schissel DN. Acrylonitrile Butadiene Styrene Polymers – Rapra Review Report 70, review report – RAPRA Technology Ltd., 1993.

Ames NM, Srivastava V, Chester S, Anand L. A thermo-mechanically-coupled theory for large deformations of amorphous polymers. Part II: applications. International Journal of Plasticity 2009;25:1495-1539.

Argon AS. A theory for the low-temperature plastic deformation of glassy polymers. Philosophical Magazine 1973;28:839–865.

Arruda EM, Boyce MC, Jayachandran R. Effects of strain rate, temperature and thermomechanical coupling on the finite strain deformation of glassy polymers. Mechanics of Materials 1995;19:193-212.

Bannantine JA, Comer JJ, Handrock JL. Fundamentals of metal fatigue analysis. USA: Prentice Hall; 1990.

Bardenhagen SG, Stout MG, Gray GT. Three-dimensional, finite deformation, viscoplastic constitutive models for polymeric materials. Mech. Mater. 1997;25:235–253.

Basquin OH. The Exponential Law of Endurance Tests. Am. Soc. Test. Mater. Proc. 1910;10:625-30.

Bernard JD, Jordon JB, Horstemeyer MF, El Kadiri H, Baird J, Lamb D, Luo AA. Structure-property relations of cyclic damage in a wrought magnesium alloy. Scr Mater. In Press, 2010.

Bernard JD, Jordon JB, Horstemeyer MF. Small fatigue crack growth observations in a wrought magnesium alloy [Under Review].

Bouvard J.L., Ward D.K., Hossain D., Nouranian S., Marin E.B., Horstemeyer M.F. Review of Hierarchical Multiscale Modeling to Describe the Mechanical Behavior of Amorphous Polymers. Jour. Eng. Matls. and Tech. 2009;131:041206.

Bowden PB, Raha S. A molecular model for yield and flow in amorphous glassy polymers making use of a dislocation analogue. Philosophical Mag. 1974;29:149-166.

Boyce MC, Parks DM, Argon AS. Large Inelastic Deformation of Glassy Polymers, Part I: Rate-Dependent Constitutive Model. Mechanics of Materials 1988;7:15-33.

Capaldi FM, Boyce MC. Enhanced Mobility Accompanies the Active Deformation of a Glassy Amorphous Polymer. Phys. Rev. Lett. 2002;89:(175505)1-4.

Chaboche JL. Thermodynamic formulation of constitutive equations and application to the viscoplasticity and viscoelasticity of metals and polymers. International Journal of Solids and Structures 1997;34:2239–2254.

Cho Ur-R. Miscibility and Properties of cis-Polybutadiene/Ethyl-Branched Polyethylene Blends (I). Korea Polymer Journal 1999;7:196-202.

Christensen RM. Theory of Viscoplasticity. Academic Press, New York 1982.

Donald AM, Kramer EJ. Plastic Deformation Mechanisms in Poly(Acrylonitrile Butadiene Styrene (ABS). Journal of Materials Science 1982;17:1765-72.

El Kadiri H, Xue Y, Horstemeyer MF, Jordon JB, Wang PT. Identification and modeling of fatigue crack growth mechanisms in a die-cast AM50 magnesium alloy. *Acta Mater* 2006;54:5061-76.

Estevez R, Tijssens MGA, Van der Giessen E. Modeling of the competition between shear yielding and crazing in glassy polymers. Journal of the Mechanics and Physics of Solids 2000;48:2585-2617.

Eyring H, Viscosity, plasticity and diffusion as examples of absolute reaction rates. Journal of Chemical Physics 1936;4:283–291.

Felton LA. Characterization of Coating Systems. *AAPS PharmSciTech*. 2007;8(4): Article 112.

Frank GJ, Brockman RA. A viscoelastic-viscoplastic constitutive model for glassy polymers. International Journal of Solids and Structures 2001;38:5149-5164.

Gall K, Horstemeyer MF, McDowell DL, Fan J. Finite element analysis of the stress distributions near damaged Si particle clusters in case Al-Si alloys. Mech Mater 2000;32(5):277-301.

Gall K, Biallas G, Maier HJ, Gullett P, Horstemeyer MF, McDowell DL, Fan J. In-Situ observations of high cycle fatigue mechanisms in cast AM60B magnesium in vacuum and water vapor environments. Int J Fatigue 2004;26:59-70.

Gibson JB, (2010) *Microstruture-Property Relationships and MultiStage Fatigue Modeling of an Extruded Magnesium AZ61 Alloy*. MS Thesis, Mississippi State University.

Govaert LE, Timmermans P, Brekelmans W. The Influence of Intrinsic Strain Softening on Strain Localization in Polycarbonate: Modeling and Experimental Validation. J. Eng. Mater. Technol. 2000;122:177-185.

Haward RN, Thackray G. The use of a mathematical model to describe isothermal stress-strain curves in glassy polymers. Proceedings of the Royal Society of London 1968;302:453–472.

Hayhurst DR, Leckie, FA, McDowell DL. Damage growth under nonproportional loading. ASTM Spec Tech Publ 1985:688-99.

Horstemeyer MF, Yang N, Gall KA, McDowell DL, Fan J, Gullett P. High cycle fatigue on a die cast AZ91E-T4 magnesium alloy Acta Mater 2004;52:1327-36.

Horstemeyer MF. Notes and Discussion 2009.

Ishikawa M., Ogawa H. Brittle fracture in glassy polymers. J. Macromol. Sci.-Phys.B19. 1981;3:421-443.

James HM, Guth E, Theory of the elastic properties of rubber. The Journal of Chemical Physics 1943;11:455–481.

Janssen R.P.M., Kanter D., Govaert L.E., Meijer H.E.H. Fatigue life predictions for glassy polymers: A constitutive approach. Macromolecules 2008;41:2520-2530.

Jordon JB, Horstemeyer MF, Yang N, Major JF, Gall KA, Fan J. Microstructural inclusion influence on fatigue of a cast A356 aluminum alloy. Metall Mater Trans A 2010;41A:356-363.

Khan AS, Zhang H, Finite deformation of a polymer: experiments and modeling. Int. J. Plasticity 2001;17:1167–1188.

Khan AS, Lopez-Pamies O, Kazmi R. Thermo-mechanical large deformation response and constitutive modeling of viscoelastic polymers over a wide range of strain rates and temperatures. Int. Journal of Plasticity 2006;22:581–601.

Kim HS, Wang XM, Nik Abdullah NAH. Effect of temperature on fatigue crack growth in the polymer ABS. Fat. Fract. Eng. Mater. Struct. 1994;17:361-67.

Konczol L., Doll W, Bevan L. Mechanisms and micromechanisms of fatigue crack propagation in glassy thermoplastics. Colloid Polymer Sci. 1990;268:814-822.

57

Krempl E. The overstress dependence of the inelastic rate of deformation inferred from transient tests. Mater. Sci. Res. Int. 1995;1:3–10.

Lawandy SN, Hepburn C. Injection Molding Temperature Effects on the Fatigue Failure of Thermoplastic Polyurethane. Elastomerics 1980a;112:45-49.

Lawandy SN, Hepburn C. Mold Temperature Effects on the Fatigue Failure of Thermoplastic Polyurethane. Elastomerics 1980b;112:24-26.

Lawandy SN, Hepburn C. Injection Molding Temperature Effects on the Fatigue Failure of Thermoplastic Polyurethane. Elastomerics 1980c;112:45-49.

Laz PJ, Hillberry BM. Fatigue life prediction from inclusion initiated cracks. Int. J. Fatigue 1998;20:263-70.

Lubarda VA, Benson DJ, Meyers MA. Strain-rate effects in rheological models of inelastic response. Int. J. Plasticity 2003;19:1097–1118.

Maiti S., Geubelle P.H. A cohesive model for fatigue failure of polymers. Eng. Fract. Mech. 2005;72:691-708.

Marissen R, Schudy D, Kemp AVJM, Coolen SMH, Duijzings WG, Van der Pol A, Van Gulick AJ.The effect of material defects on the fatigue behavior and the fracture strain of ABS. Jour. Mat. Sci. 2001;36:4167-80.

McClintock FA. Considerations for fatigue crack growth relative to crack tip displacement. In: Bynon JH, Brown MW, Lindley TC, Smith RA, Tomkins B, editors. Engineering Against Fatigue. Balkema press: 1999. P. 227‑41 [chapter 24].

McDowell DL, Gall K, Horstemeyer MF, Fan J. Microstructure-based fatigue modeling of cast A356-T6 alloy. Eng Fract Mech 2003;70:49-80.

McEvily A.J., Boettner R.C., Johnston T.L. On the Formation and Growth of Fatigue Cracks in Polymers. Proceedings of the 10th Sagamore AMR Conference, Syracuse 1964:95.

Mulliken AD, Boyce MC. Mechanical of rate-dependent elastic-plastic deformation of glassy polymers from low to high strain rate. International Journal of Solids and Structures 2005;43:1331-56.

Mulliken AD, Boyce MC. Polycarbonate and Polycarbonate-POSS Nanocomposites at High Rates of deformation. Journal of Engineering Materials and Technology 2006;128:543-550.

Newman JA, Willard SA, Smith SW, Piascik RS. Replica-based Crack Inspection. Eng. Fract. Mech. 2009;76:898-910.

Perzyna P. Fundamental problems in viscoplasticity. In: Advances in Applied Mechanics vol. 9. Academic Press, New York, pp. 243–377.

Pijnenburg K.G.W., Steenbrink A.C., Van der Giessen E. Shearing of particles during crack growth in polymer blends. Polymer 1999;40:5761-71.

Pitman G, Ward IM. Molecular weight dependence on the fatigue crack propagation in polycarbonate. Journal of Materials Science 1980;15:635-45.

Qi H.J., Boyce M.C. Stress-strain behavior of thermoplastic polyurethanes. Mechanics of Materials. 2004; 37:817-39.

Radon J.C. Fatigue crack growth in polymers. Int. Journal of Fract. 1980;16:533-52.

Richeton J, Ahzi S, Vecchio KS, Jiang FC, Adharapurapu RR. Influence of temperature and strain rate on the mechanical behavior of three amorphous polymers: Characterization and modeling of the compressive yield stress. International Journal of Solids and Structures 2006;43:2318–2335.

Seelig T., van der Giessen E. Localized plastic deformation in ternary blends. Int. Jrnl. Of Solids and Struct. 2002;39:3505-22.

Shiozawa K, Tohda Y, Sun S-M. Crack Initiation and Small Fatigue Crack Growth Behaviour of Squeeze-cast Al-Si Aluminum Alloys. Fat. Fract. Engng Mater. Struct. 1997;20:237-47.

Sikka S. Some Observations on Fatigue and Crazing of Polycarbonate (Bishenol A). Polymer Bulletin 1980;3:61-68.

Suresh S. Fatigue of materials. 2nd ed. Cambridge: Cambridge University Press; 2003.

Tervoort T, Smith R, Brekelmans W, Govaert L. A Constitutive Equation for the Elasto-Viscoplastic Deformation of Glassy Polymers. Mech. Time Mater. 1998;1:269-291.

Tervoort TA, Govaert LE. Strain-hardening behavior of polycarbonate in the glassy state. J. Rheol. 2000;44:1263-1277.

Tijssens M.G.A., van der Giessen E., Sluys L.J. Modeling of crazing using a cohesive surface methodology. Mech. of Matls. 2000;32:19-35.

Van der Giessen E., Estevez R., Pijnenburg K.G.W., Tijssens M.G.A. Computational modeling of failure processes in polymers. European Conference on Computational Mechanics 1999.

Van der Sluis O, Schreurs PJG, Meijer HEH. Homogenisation of structured elastoviscoplastic solids at finite strains. Mech. Of Mater., 2001;33:499–522.

Weiland H., Nardiello J., Zaefferer S., Cheong S., Papzian J., Raabe D. Microstructural aspects of crack nuclaeation during cyclic load of AA7075-T651. Eng. Fract. Mech. 2009;76:709-714.

Williams J.G. A model of fatigue crack growth in polymers. Journal of Mat. Sci. 1977;12:2525-33.

Xue Y, Horstemeyer MF, McDowell DL, El Kadiri H, Fan J. Microstructure-based multistage fatigue modeling of a cast AE44 magnesium alloy. Int J Fatigue 2007a;29:666-76.

Xue Y, Burton CL, Horstemeyer MF, McDowell DL, Berry JT. Multistage fatigue modeling of cast A356-T6 and A380-F aluminum alloys. Metall Mater Trans B 2007b;38B:601-6.

Xue Y, El Kadiri H, Horstemeyer MF, Weiland H. Micromechanisms of multistage fatigue crack   growth in a high-strength aluminum alloy. *Acta Mater* 2007c;*55:*1975-84.

Xue Y, McDowell DL, Horstemeyer MF, Dale MH, Jordon JB. Microstructure-based multistage fatigue modeling of aluminum alloy 7075-T651. Eng Fract Mech 2007d;74:2810-23.

Xue Y, Pascu A, Horstemeyer MF, Wang L, Wang PT. Microporosity effects on cyclic plasticity and fatigue of LENS-processed steel. Acta Mater 2010;58:4029-38.

Zaïri, F, Naït-Abdelaziz M, Woznica K, Gloaguen JM. Elasto-viscoplastic constitutive equations for the description of glassy polymers behavior at constant strain rate. JEMT 2007;129:29-35.